Global Change Biology (2006) **12,** 2370–2390, doi: 10.1111/j.1365-2486.2006.01254.x

The contributions of land-use change, CO_2 fertilization, and climate variability to the Eastern US carbon sink

MARCO ALBANI*, DAVID MEDVIGY*, GEORGE C. HURTT† and PAUL R. MOORCROFT*
*Department of Organismic and Evolutionary Biology, Harvard University, 22 Divinity Avenue, Cambridge, MA 02138, USA,
†Institute for the Study of Earth Oceans and Space, University of New Hampshire, Durham, NH 03824, USA

Abstract

Atmospheric measurements and land-based inventories imply that terrestrial ecosystems in the northern hemisphere are taking up significant amounts of anthropogenic carbon dioxide (CO_2) emissions; however, there is considerable disagreement about the causes of this uptake, and its expected future trajectory. In this paper, we use the ecosystem demography (ED) model to quantify the contributions of disturbance history, CO_2 fertilization and climate variability to the past, current, and future terrestrial carbon fluxes in the Eastern United States. The simulations indicate that forest regrowth following agricultural abandonment accounts for uptake of 0.11 Pg C yr^{-1} in the 1980s and 0.15 Pg C yr^{-1} in the 1990s, and regrowth following forest harvesting accounts for an additional 0.1 Pg C yr^{-1} of uptake during both these decades. The addition of CO_2 fertilization into the model simulations increases carbon uptake rates to 0.38 Pg C yr^{-1} in the 1980s and 0.47 Pg C yr^{-1} in the 1990s. Comparisons of predicted aboveground carbon uptake to regional-scale forest inventory measurements indicate that the model's predictions in the absence of CO_2 fertilization are 14% lower than observed, while in the presence of CO_2 fertilization, predicted uptake rates are 28% larger than observed. Comparable results are obtained from comparisons of predicted total Net Ecosystem Productivity to the carbon fluxes observed at the Harvard Forest flux tower site and in model simulations free-air CO_2 enrichment (FACE) experiments. These results imply that disturbance history is the principal mechanism responsible for current carbon uptake in the Eastern United States, and that conventional biogeochemical formulations of plant growth overestimate the response of plants to rising CO_2 levels. Model projections out to 2100 imply that the carbon uptake arising from forest regrowth will increasingly be dominated by forest regrowth following harvesting. Consequently, actual carbon storage declines to near zero by the end of the 21st century as the forest regrowth that has occurred since agricultural abandonment comes into equilibrium with the landscape's new disturbance regime. Incorporating interannual climate variability into the model simulations gives rise to large interannual variation in regional carbon fluxes, indicating that long-term measurements are necessary to detect the signature of processes that give rise to long-term uptake and storage.

Keywords: climate variability, CO_2 fertilization, CO_2 fluxes, disturbance history, Eastern United States, ecosystem demography (ED) model, forest harvesting, land-use history, regional-scale uptake, terrestrial carbon sink

Received 26 January 2006 and accepted 28 March 2006

Introduction

Atmospheric measurements and land-based inventories indicate that northern temperate ecosystems are absorbing a sizeable fraction of the carbon dioxide (CO_2) emitted by fossil fuel burning (Pacala *et al*., 2001). This uptake has been attributed to two qualitatively different sets of mechanisms. The first set of mechanisms attribute carbon uptake to enhanced forest growth arising from CO_2 fertilization, nitrogen deposition and climate change (Schimel, 1995; Cao & Woodward, 1998;

Correspondence: Paul R. Moorcroft, fax + 1 617 495 9484,
e-mail: paul_moorcroft@fas.harvard.edu

Kicklighter *et al*., 1999; Joos *et al*., 2001, 2002; McGuire *et al*., 2001). The second set of mechanisms attribute the sink to disturbance history – forest regrowth that is occurring as a result of agricultural land abandonment, forest harvesting and fire suppression (Houghton *et al*., 1999; Caspersen *et al*., 2000; Schimel *et al*., 2000; McGuire *et al*., 2001; Hurtt *et al*., 2002; Goodale *et al*., 2002; Houghton, 2003; Nabuurs *et al*., 2003).

While there is general agreement that the contributions of enhanced plant growth arising from nitrogen fertilization and changes in climate to current patterns of US carbon uptake are relatively small (Schimel *et al*., 2001), there is continuing disagreement about whether CO_2 fertilization or disturbance history is the dominant mechanism responsible for carbon uptake by US ecosystems (Joos *et al*., 2002; Houghton, 2003). A detailed study involving four terrestrial biosphere models (McGuire *et al*., 2001) emphasized CO_2 fertilization as the primary mechanism responsible for carbon uptake in US ecosystems, as well as the rest of the globe. Carbon accounting and integrated assessment model studies (Houghton *et al*., 1999; Houghton, 2003; Jain and Yang, 2005) have reached similar conclusions, implying that CO_2 fertilization is responsible for up to 80% of carbon uptake in the United States. In contrast, empirical analyses of forest inventory data (Birdsey & Heath, 1995; Brown *et al*., 1997; Caspersen *et al*., 2000; Pacala *et al*., 2004), and modeling studies by Schimel *et al*. (2001), Hurtt *et al*. (2002) have emphasized the role of forest regrowth arising from agricultural abandonment, forest harvesting and fire suppression as the dominant mechanism responsible for carbon uptake (though see Joos *et al*., 2002).

Quantifying the contributions of these different mechanisms to the patterns of uptake over recent decades is important as the mechanisms have markedly different implications for magnitude of uptake over the coming decades. In particular, if CO_2 uptake is arising primarily from a CO_2-related enhancement of plant growth, this may continue and may even increase as atmospheric CO_2 levels continue to rise. In contrast, if the sink is primarily arising as a result of the legacy of agricultural abandonment during the late 19th and early 20th century, the sink will saturate as forests regain their former biomass and soil carbon. Assessing the relative contribution of disturbance history and ecophysiological responses to the current pattern of CO_2 fluxes is, therefore, critical to predicting the expected rates of CO_2 uptake over the next century (Hurtt *et al*., 2002; Houghton, 2003).

In this study, we use a new parameterization of the ecosystem demography (ED) model for the Eastern United States in conjunction with a new, high-resolution land use change dataset and forest-harvesting scenario to quantify the relative contributions of land-use change, forest harvesting, CO_2 fertilization and climate variability to the carbon fluxes of the ecosystems of the Eastern United States. A unique feature of the ED model is its use of a system of size- and age-structured partial differential equations to explicitly track the subgrid scale ecosystem heterogeneity arising from subgrid scale disturbances such as forest harvesting and land abandonment (Moorcroft *et al*., 2001; Hurtt *et al*., 2002). In contrast to previous modeling studies, the model's predictions of carbon uptake and storage are directly evaluated against regional measurements of long-term aboveground carbon accumulation obtained from the US Forest Service Forest Inventory Analysis (FIA) program and site-level measurements of CO_2 fluxes at the Harvard Forest flux tower.

Materials and methods

ED model

The ED model (Moorcroft *et al*., 2001; Hurtt *et al*., 2002) is a terrestrial ecosystem model that uses the following system of size- and age-structured partial differential equations to approximate the behavior of an individual-based, stochastic gap model:

$$\underbrace{\frac{\partial}{\partial t}C_i(\mathbf{z},a,t)}_{\text{change in plant density}} = \underbrace{-\nabla_{\mathbf{z}}[g(\mathbf{z},\mathbf{r},t)\,C_i(\mathbf{z},a,t)]}_{\text{plant growth}} \underbrace{-\mu(\mathbf{z},\mathbf{r},t)\,C_i(\mathbf{z},a,t)}_{\text{mortality}} \underbrace{-\nabla_a C_i(\mathbf{z},a,t)}_{\text{aging of plant community}}. \quad (1)$$

$$\underbrace{\frac{\partial}{\partial t}p(a,t)}_{\text{change in landscape age structure}} = \underbrace{-\nabla_a \cdot p(a,t)}_{\text{aging}} - \underbrace{\lambda(a,t)p(a,t)}_{\text{disturbance}}, \quad (2)$$

where

$$\nabla_{\mathbf{z}} = \left\{\frac{\partial}{\partial z_s}, \frac{\partial}{\partial z_a}\right\}, \quad \nabla_a = \left\{\frac{\partial}{\partial a}\right\}, \quad \int_0^\infty p(a,t)\,\mathrm{d}a = 1.$$

Equation (1) describes changing distribution of plant biomass within each grid cell, where $\mathbf{z}$ is the array of structural (z_s) and live biomass (z_a) compartment sizes (units: kg C); $C_i\,(\mathbf{z},a,t)\,\mathrm{d}\mathbf{z}\,\mathrm{d}a$ is the biomass density (units: kg C m^{-2}) of plants of type i and size $\mathbf{z}$ in places disturbed a years ago at time t; $\mathbf{r}$ is a vector describing the resource environment (light, water, nitrogen) experienced by an individual of size $\mathbf{z}$; $g(\mathbf{z},\mathbf{r},t)$ is the rate at which the structural and live biomass of a plant of size $\mathbf{z}$ in environment $\mathbf{r}$ increase (units: kg C yr^{-1}); and $\mu\mathrm{mol},\mathbf{r},t)$ is the per capita rate of tree mortality (units:

year^{-1}). Equation (2) describes the changing dynamical distribution of landscape ages within each grid cell arising from disturbance events, where $p(a) \cdot da$ is the fraction of the grid–cell disturbed between a and $a + da$ years ago, and $\lambda(a, t)$ is the rate of disturbance (units: year^{-1}).

Equations (1) and (2) are linked through boundary conditions. The recruitment of new seedlings f_i $(\mathbf{z}, a, t)$ corresponds to a flux of individuals into the system at $(\mathbf{z}_0, a)$. Under the assumption of random dispersal of seeds between gaps within a grid cell this yields the following boundary condition:

$$C_i(\mathbf{z_0}, a, t) = \underbrace{\frac{\int_0^\infty \int_{\mathbf{z}_{0s}}^\infty \int_{\mathbf{z}_{0a}}^\infty C_i(\mathbf{z}, a, t) f_i(\mathbf{z}, a, t) p(a, t)\, \mathrm{d}z_a\, \mathrm{d}z_s\, \mathrm{d}a}{g_{i,a}(\mathbf{z}_0, \mathbf{r}, t) + g_{i,s}(\mathbf{z}_0, \mathbf{r}, t)}}_{\text{recruitment}}. \quad (3)$$

Equation (1) has also a second boundary condition describing the state of the ecosystem after a disturbance event

$$\underbrace{C_i(\mathbf{z}, 0, t) = \int_0^\infty s_i(\mathbf{z}, a, t) p(a, t)\, \mathrm{d}a}_{\text{plant community following disturbance event}}, \quad (4)$$

where the function $s_i(\mathbf{z}, a, t)$ describes the survivorship of individuals of size $\mathbf{z}$ and type i following the disturbance. Equation (2) also has the following boundary condition describing the formation of newly disturbed areas within the grid cell

$$\underbrace{p(0, t) = \int_0^\infty \lambda(a, t)\, p(a, t)\, \mathrm{d}a}_{\text{formation of newly disturbed areas}}. \quad (5)$$

These equations for aboveground ecosystem dynamics are coupled to belowground equations that track water availability and carbon and nitrogen decomposition in the soil (see Appendix A). With this system of equations, the ED model is able to incorporate both the effects of physiological responses of vegetation to atmospheric forcing, and the effects of disturbance history on long-term vegetation dynamics and ecosystem biogeochemistry (Hurtt *et al*., 1998; Moorcroft, 2003).

The general structure of the ED model used in this study is the same as that in Moorcroft *et al*. (2001), however, a number of modifications were made to capture (i) the composition and structure of Eastern North American ecosystems, and (ii) the impact of land-use transitions and forest harvesting on ecosystem structure and fluxes.

Plant Functional Types (PFTs)

Seven new PFTs, differing in their leaf physiology, allometry, mortality and dispersal, were parameterized from empirical data to represent the range of plant life histories found within the region: three deciduous, broad-leaved tree types (early-, mid-, and late-successional), three coniferous tree types (southern pines, northern pines and late successional conifers), and a C_3 forbs PFT. At the level of leaf physiology, the PFTs exhibit correlated differences in their specific leaf area and their photosynthetic rate per unit leaf area (Vm_0) (Table 1). The differences in Vm_0 determine three important functional characteristics of the PFTs: the maximum rate of photosynthesis per unit leaf area, the PFT compensation point for light, and the PFT's density-dependent mortality rate. The first two derive directly from the formulation of the Farquhar *et al*. (1980) model of leaf photosynthesis; the third is a consequence of the way mortality is computed in ED, in which a plant's mortality varies as a function of its carbon balance. High Vm_0 species are shade-intolerant with high rates of leaf-level gross primary productivity (GPP) in full light, but have a higher compensation point for light, and thus higher levels of mortality in the understory; low Vm_0 species are shade tolerant, with lower rates of leaf-level GPP in full light, but have a lower compensation point for light, and thus a lower mortality rate in the understory.

The PFTs also varied in their growth, mortality and recruitment life-history characteristics. height-to-diameter at breast height (DBH), structural biomass-to-DBH, and leaf biomass-to-DBH relationships for each PFT were specified from empirical allometry estimates (Table 2), and density-independent mortality rates for each PFT were specified from forest inventory measurements. With respect to recruitment, empirical data from representative species for each PFT used to parameterize differences in seed dispersal characteristics and the sensitivity of seedlings to frost-induced mortality. Details of these parameterizations can be found in Appendix B.

Incorporating disturbance history

A unique feature of the ED model is its ability to track the changing landscape age structure and associated subgrid scale heterogeneity in environmental conditions that arises from prior disturbance history of ecosystems. The original ED formulation used Eqn (2) to track subgrid scale ecosystem heterogeneity arising from a single mode of natural disturbance. Here, following the approach of Hurtt *et al*. (2002), Eqn (2) is generalized to track ecosystem heterogeneity arising

Table 1 Ecophysiological and life-history parameters for the plant functional types

PFT	Leaf habit*	Vm_0 ($\mu mol\,m^{-2}\,s^{-1}$)	SLA ($m^2\,kg\,C^{-1}$)	Leaf N content ($g\,C\,m^{-2}$)	Density independent mortality rate ($year^{-1}$)	Minimum temperature (°C)	Global dispersal (fraction)
C_3 Grasses/Forbs (G)	DD/CD	18.25	11	3.46	1.0	−80	1.0
Northern pines (NP)	E	15.625	3	2.98	0.01	−80	0.78
Southern pines (SP)	E	15.625	4.5	2.98	0.01	−5	0.78
Late successional conifers (LSC)	E	6.25	5	1.25	0.005	−60	0.001
Early successional hardwoods (ESD)	CD	18.25	20	3.46	0.067	−80	1.0
Late successional hardwoods (LSD)	CD	6.25	30	1.26	0.011	−20	0.074
Mid successional hardwoods (MSD)	CD	15.625	15	2.98	0.059	−20	0.32

*CD, cold deciduous; DD, drought deciduous; E, Evergreen.

Table 2 Allometric parameters of the six woody plant functional types. Northern pines and southern pines share the same allometric equations

PFT	Leaf biomass equation	Structural biomass equation	Height–DBH equation
Early successional hardwoods (ESD) e.g.: *Betula lenta*,	$a_l = 0.0047$	$a_s = 0.0265$	$b_{1h} = 22.68$
B. papyrifera and *Populus* spp.	$b_l = 2.249$	$b_s = 2.959$	$b_{2h} = -0.0653$
Northern pines (NP) and southern pines (SP)	$a_l = 0.024$	$a_s = 0.147$	$b_{1h} = 27.14$
e.g.: *Pinus strobus*, *P. banksiana*, *P. taeda* and *P. resinosa*	$b_l = 1.899$	$b_s = 2.238$	$b_{2h} = -0.0388$
Late successional conifers (LSC) e.g.: *Picea* spp., *Tsuga canadiensis*	$a_l = 0.045$	$a_s = 0.1617$	$b_{1h} = 22.79$
	$b_l = 1.683$	$b_s = 2.1536$	$b_{2h} = -0.0445$
Late successional hardwoods (LSD) e.g.: *Fagus grandifolia* and *A. saccharum*	$a_l = 0.017$	$a_s = 0.235$	$b_{1h} = 23.39$
	$b_l = 1.731$	$b_s = 2.252$	$b_{2h} = -0.0540$
Mid successional hardwoods (MSD) e.g.: *Quercus alba* and *Acer rubrum*	$a_l = 0.024$	$a_s = 0.148$	$b_{1h} = 25.18$
	$b_l = 1.860$	$b_s = 2.411$	$b_{2h} = -0.0496$

from multiple modes of disturbance

$$\underbrace{\frac{\partial}{\partial t}\mathbf{p}(a,\,t)}_{\text{ch. in land class age distribution}} = \underbrace{-\frac{\partial}{\partial a}\mathbf{p}(a,\,t)}_{\text{aging}} - \underbrace{\Lambda(a,\,t)\mathbf{p}(a,\,t)}_{\text{disturbance}}, \tag{6}$$

where $\mathbf{p}(a)$ is a vector whose elements $[p_1(a), p_j(a), \ldots p_m(a)]$ describe the distributions of times since disturbance for each of the m land-use states represented in the model, and $\Lambda(a,\,t)$ is a $m \times m$ matrix whose elements describe the disturbance history forcing – the rate at which land transitions between the different land use states as function of time and age (time since last disturbance). Equation (6) has the following boundary condition describing the formation of new areas within each land-use state:

$$\underbrace{p_j(0,\,t) = \sum_k^m \int_0^\infty \lambda(a,\,t) p_k(a,\,t)\,\mathrm{d}a}_{\text{formation of newly disturbed areas}} \quad (j=l,\,\ldots,\,m). \tag{7}$$

Equation (6) is also subject to the following integral constraint:

$$\sum_{j=1}^{m} \int_0^\infty p_j(a,\,t)\,\mathrm{d}a = 1. \tag{8}$$

Further details on the how disturbance forcing scenario is calculated are given in 'Analysis'.

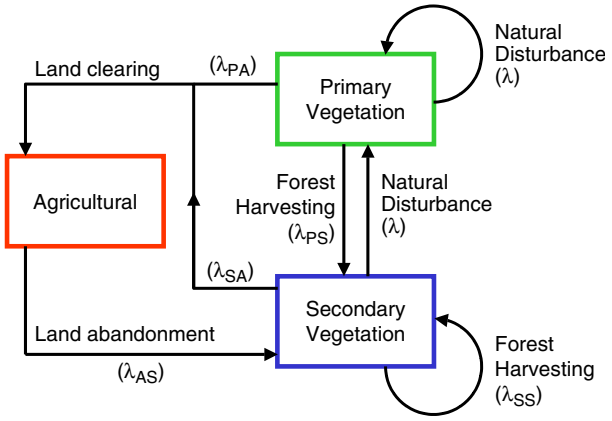

Fig. 1 Schematic illustrating how disturbance history forcing is applied to the ecosystem demography simulations using Eqns (6)–(9). Land clearing for agricultural uses removes land from primary and secondary vegetation at rates λ_{PA} and λ_{SA}, respectively; abandoned agricultural land is colonized by secondary vegetation at rate λ_{AS}, and is transferred to primary vegetation by natural disturbance at rate λ; forest harvesting affects both secondary and primary vegetation at rates λ_{SS} and λ_{PS}, respectively. Harvested patches are colonized by secondary vegetation.

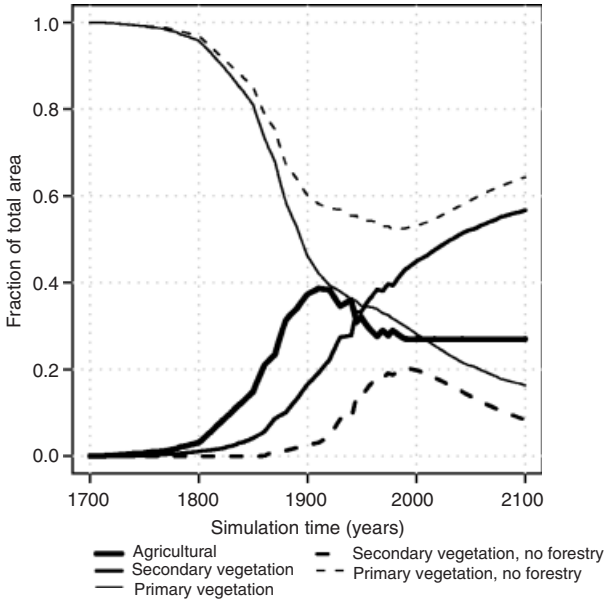

Fig. 2 Land-use changes in the Eastern United States in the presence of forest harvesting, and when forest harvesting is neglected (dotted lines). Land-use change is not projected beyond the present date, while forest harvesting rates are projected based on USDA estimates.

Analysis

The contributions of land-use change, forest harvesting, and CO_2 fertilization to the carbon fluxes of the Eastern United States were quantified by simulating the terrestrial ecosystem dynamics of the continental United States east of 100°W for the period 1700–2100, progressively adding the following sources of forcing: (i) historical land-use change, (ii) historical and projected forest harvesting and (iii) historical and projected changes in atmospheric CO_2 concentrations. The simulations were repeated imposing variable climate for the years 1948–2002 to investigate the impact of interannual variability in climate on the model's predictions.

Disturbance history forcing

In this analysis, we incorporated three land-use states: primary vegetation, secondary vegetation and agricultural land, with each land-use state being defined by last form of disturbance that occurred in a particular place. The transitions between the three land-use states were as follows: agricultural clearing converts primary and secondary vegetation to agricultural land; agricultural abandonment converts agricultural land to secondary vegetation; forest harvesting of either primary or secondary vegetation converts harvested areas to secondary vegetation; and natural disturbance in either primary or secondary vegetation converts the disturbed area to primary vegetation (Fig. 1).

Mathematically this corresponds to $\mathbf{p}(a,\ t) = [p_P(a,t), p_S(a,t),\ p_A(a,t)]$, where $p_P(a,t)$, $p_S(a,t)$ and $p_A(a,t)$ are, respectively, the age distributions of primary, secondary and agricultural lands at time t, and $\Lambda(a,t)$ having the following form:

$$\Lambda(a,\ t) = \begin{pmatrix} \lambda & \lambda & 0 \\ \lambda_{PS} & \lambda_{SS} & \lambda_{AS} \\ \lambda_{PA} & \lambda_{SA} & 0 \end{pmatrix}. \qquad (9)$$

Where the time and age dependencies of the matrix elements have been omitted for notational compactness. The different types of disturbance transitions (λ, λ_{PS}, λ_{SS}, λ_{AS}, λ_{PA} and λ_{SA}) differ in both the rates at which they occur, and in their intensity – the impact of the transition on the above-ground and belowground ecosystem. The transitions rates to (λ_{PA}, λ_{SA}), and from (λ_{AS}), the agricultural land class were specified from (i) from the Waisanen & Bliss (2002) historical county-level land-use dataset for the period 1850-present, and (ii) Ramankutty & Foley's (1999) $1^\circ \times 1^\circ$ resolution dataset on the historical fractions of agricultural land for the period 1700–1850 (Fig. 2). The rates of forest harvesting (λ_{PS}, λ_{SS}) were specified to match historical and projected rates of wood production shown in Fig. 3. The frequency of natural canopy gap formation on primary and secondary lands (λ) was 0.01 year^{-1} on areas older than 50 years, yielding an average rate of canopy gap formation

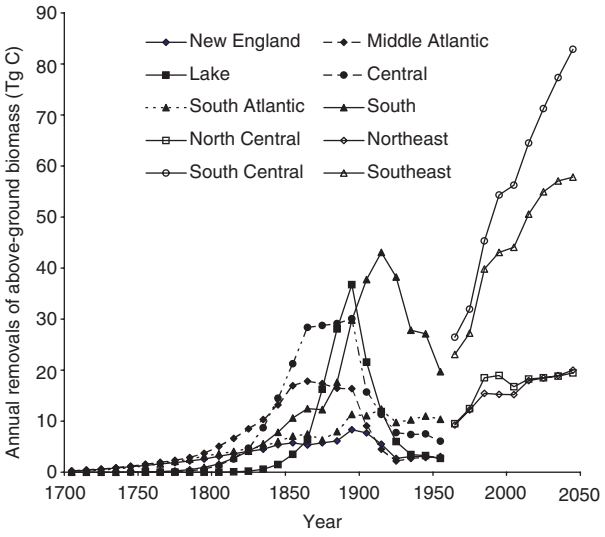

Fig. 3 Total annual harvesting of aboveground biomass by region: different regions are used for 1700–1959 and 1960–2100. Most regions show a decline in harvesting in the first half of the 20th century as fossil fuels replace wood as heating source, and as a larger proportion of the lumber demand is met by western forests.

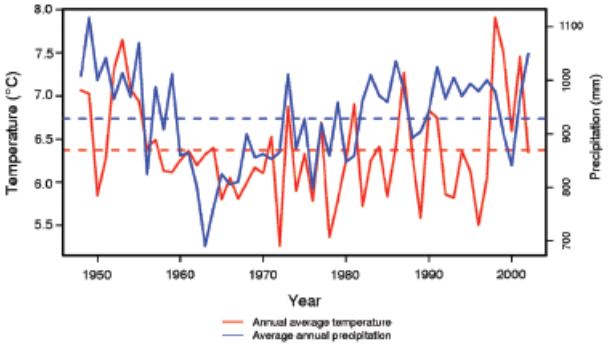

Fig. 4 Annual average temperature and precipitation for the simulation domain in the period 1948–2002 as obtained from the NCEP 2.5° data grid. Horizontal dotted lines represent the average for the period. There is substantial temporal autocorrelation in the precipitation anomalies, with a wetter decade (1948–1959) followed by two drier ones (1960–1981) and then two wetter ones (1982–2002) while temperature is less temporally autocorrelated.

of 0.007 year^{-1} – a value consistent with the US Forest Service's FIA dataset for the Eastern United States (P. R. Moorcroft, unpublished results). The disturbance scenario was projected forward to 2100 under the assumption that (i) the fraction of agricultural land will remain constant (i.e. after 2002, λ_{PA}, λ_{SA} and $\lambda_{AS} = 0$ in Eqn (9)), and (ii) biomass harvesting rates were projected to 2050 using USDA projection estimates (Haynes, 2003), and then maintained at these rates until 2100.

The impact of the different disturbance transitions on ecosystem structure and fluxes is defined by Eqn (4), which describes the state of the ecosystem following each type of land-use transition. In areas where natural canopy-gap formation occurs, the aboveground biomass of the standing vegetation is transferred to the decomposition model; in areas that transition into agriculture, all aboveground structural biomass is removed, foliar and root biomass is transferred into the decomposition model, and the areas are planted with C_3 forbs and grasses; abandoned agricultural areas that transition into secondary vegetation are opened to natural colonization by the different PFTs in the model; in forested areas that are harvested, all aboveground structural biomass is removed, foliar and root biomass is transferred to the decomposition model, and, depending on year and region, harvested areas are either left open to natural regeneration or planted with pines. Further details on the disturbance history scenario can be found in Appendix C.

Environmental forcing

Simulations were performed at both preindustrial atmospheric CO_2 concentrations of 280 ppm, and using the IPCC IS92a CO_2 fertilization scenario (IPCC, 1998). Hourly temperature, humidity, radiation and precipitation drivers for each grid cell were specified as the average of the 1948–2002 climate from the nearest 2.5° resolution NCEP/NCAR Reanalysis 1 data (Kalnay *et al.*, 1996; Kistler *et al.*, 2001). In the variable climate model simulations, the yearly NCEP/NCAR Reanalysis 1 data were used for the 1948–2002 period (Fig. 4), and the average climate for the 1700–1947 and 2003–2100 periods.

All modeling experiments were run from a precolonization equilibrium 'potential vegetation' initial condition, obtained by initializing the model with 0.1 saplings m^{-2} of each PFT in every site, and performing a 700-year model integration under average NCEP climate and preindustrial CO_2 concentrations of 280 ppm. Each grid cell was initialized with 2 kg m^{-2} of inorganic nitrogen with no further additions or losses.

Results

The results of the 700-year model integration to the precolonization potential vegetation equilibrium is shown in Fig. 5. While forest inventory data are not available for a detailed evaluation of this precolonization state, the simulations yielded a reasonable equilibrium spatial distribution of aboveground biomass (Fig. 5a). The average aboveground biomass is 103 Mg C ha^{-1} in the

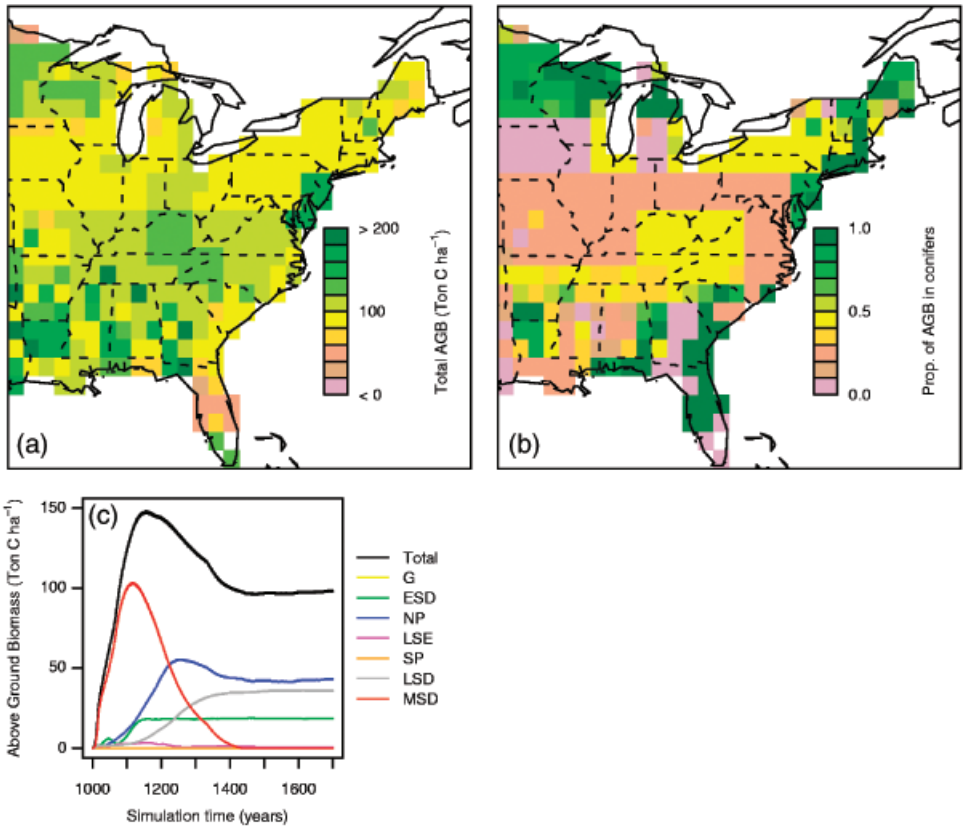

Fig. 5 Ecosystem demography model prediction of (a) presettlement vegetation aboveground biomass (tC ha^{-1}) and (b) fraction of the aboveground biomass in conifer plant functional types (PFTs) after 700-year initialization run starting from an initial condition of a few seedlings in each grid cell. The Gulf coast and eastern Texas are dominated by the broad-leaved PFT that are functionally evergreen. (c) Dynamics of aboveground biomass (tC ha^{-1}) during the 700 year initialization run for a grid cell in central Massachusetts.

northeast, 96 Mg C ha^{-1} in the Great Lakes region, 104 Mg C ha^{-1} in the southeast and 107 Mg C ha^{-1} in the south. Note that these grid-cell level values are the average over all age classes, and thus do not represent values that one would expect in old-growth stands, but rather are the values expected for forested areas subject to the natural background disturbance. The model also captures the expected general trend of northern and southern dominance of coniferous PFTs, with hardwoods dominating in the central latitudes (Fig. 5b). This pattern arises from changes in competitive balance between the PFTs with coniferous trees having an advantage of winter photosynthesis in the south and lower frost-induced mortality in the north. Subgrid heterogeneity in ecosystem composition is maintained by the gap-age gradient in light availability, with most sites equilibrating with between two and four PFTs: early and mid-successional PFTs dominate young gaps, and mid-or late-successional PFTs dominate in older gaps. An example of the precolonization subgrid scale ecosystem composition is shown in Fig. 5c.

Figure 6 shows the spatial patterns of subgrid scale land use that arise from the dynamics of land-use transitions and forest harvesting. Up until 1850, agricultural clearing is restricted to the coastal states and the Ohio valley, and primary vegetation dominates west of the Missouri river and in most of the south (Fig. 6b). By 1900, the picture has changed substantially, with most of the primary vegetation converted to agriculture in the mid-west and the Lake states, increased agricultural use and forest harvesting in the southern Atlantic states, and an increase in secondary vegetation in the northeast due to agricultural abandonment and forest harvesting (Fig. 6c). From 1900 to 1950, increased forest harvesting increases the fraction of secondary vegetation in the south (Fig. 6d and e), and between 1975 and 2050, historical and projected rates of forest harvesting increase in all regions, but especially in the south and south-east (Fig. 6f–i).

The resulting patterns of aboveground biomass in the year 2000 that arise from this disturbance forcing are shown in Fig. 7. Aboveground biomass (Fig. 7a) is

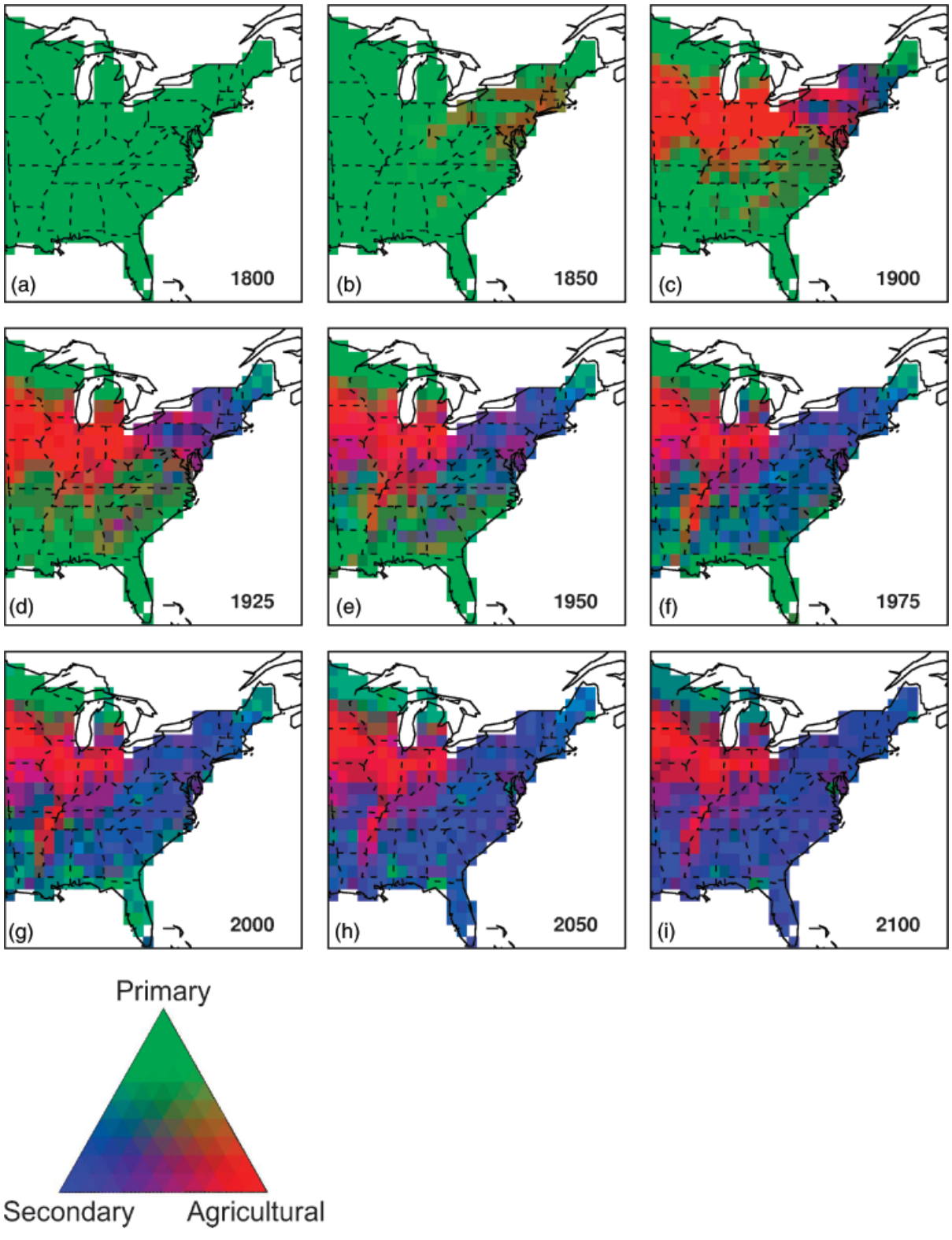

Fig. 6 Subgrid scale distribution of land-use types at selected years under the land-use plus forest-harvesting scenario. The fractions of primary, secondary and agricultural land within each grid cell are indicated by the intensity of green, blue and red coloration (see legend). The panels show clearly the western expansion of agriculture between 1850 and 1900, and the subsequent abandonment of agriculture in New England and in the Atlantic states.

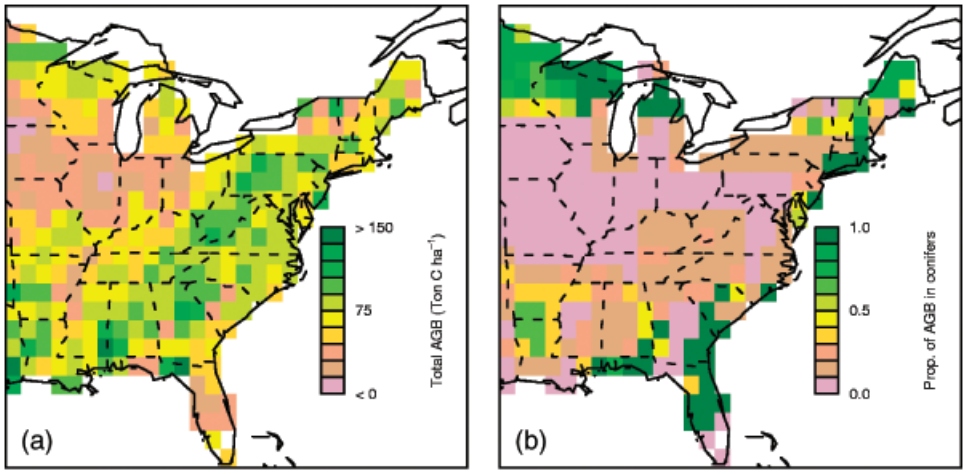

Fig. 7 Ecosystem demography model predictions of (a) aboveground biomass ($tC\,ha^{-1}$), and (b) fraction of the aboveground biomass in coniferous plant functional types in year 2000 after forcing the model with the land-use and forest harvesting history shown in Fig. 6.

substantially lower than it was at the beginning of the simulation as a consequence of both decreases in forest area and the reduced average forest age. The fraction of aboveground biomass in conifers also decreases substantially throughout the central latitudes, as the abandoned agricultural fields and recently disturbed areas have been occupied by early and mid-successional hardwoods (Fig. 7b).

Figure 8 shows the spatio-temporal patterns of carbon uptake (net ecosystem productivity, NEP) that result from the spatial and temporal patterns of land-use transitions and forest harvesting shown in Fig. 6. In 1800, the region is in approximate carbon balance (Fig. 8a), but by 1850, New England, the mid-Atlantic states, and parts of the Ohio Valley are showing carbon loss rates of $\sim 1.5\,tC\,ha^{-1}\,yr^{-1}$ as forests are cleared for agriculture (Fig. 8b). By 1900, the losses of carbon shift to the mid-west due to the westward migration of agriculture, with annual loss rates of up to $3\,tC\,ha^{-1}\,yr^{-1}$ (Fig. 8c). By 1925, New England has switched from carbon loss to carbon uptake due to the regrowth of secondary forests on abandoned agricultural land, with carbon uptake rates between 0.5 and $1.5\,tC\,ha^{-1}\,yr^{-1}$ (Fig. 8d). By 1975, the mid-Atlantic and Southern states are also taking up carbon due to forest regrowth on abandoned agricultural lands, and following forest harvesting with uptake rates in excess of $1.5\,tC\,ha^{-1}\,yr^{-1}$ (Fig. 8f). By 2000, the highest rates of carbon uptake are in the south reflecting forest regrowth following harvesting, but high rates of uptake continue to occur across the mid-Atlantic region as forest regrowth on abandoned agricultural lands continues (Fig. 8g). Over the 21st century, the spatial distribution of uptake shifts toward the south, as the effects of recovery from agriculture decline in the New England and the mid-Atlantic states, and regional uptake is increasingly dominated by forest regrowth following harvesting (Fig. 8h and i).

Summing the above fluxes across the simulation domain indicates that the region is a net source of carbon to the atmosphere for the first 250 years (Fig. 9a), reaching a peak loss rate of carbon uptake of $-0.27\,Pg\,C\,yr^{-1}$ in the 1890s, and then switching from net carbon release to net carbon uptake in the 1950s. The magnitude of the carbon uptake then increases over the next decades with an uptake rate of $0.21\,Pg\,C\,yr^{-1}$ in the 1980s, $0.25\,Pg\,C\,yr^{-1}$ in the 1990s and reaching a peak uptake rate of $0.26\,Pg\,C\,yr^{-1}$ in 2008. Regional uptake is then maintained throughout the rest of the 21st century, at $\sim 0.25\,Pg\,C\,yr^{-1}$.

Excluding the effects of forest harvesting substantially alters the pattern and magnitude of the carbon fluxes. Before 1900, carbon uptake rates are relatively unchanged, but after 1900, the absence of forest harvesting reduces the rates of carbon uptake from 0.21 to $0.11\,Pg\,C\,yr^{-1}$ in the 1980s, and from 0.25 to $0.14\,Pg\,C\,yr^{-1}$ in the 1990s (Fig. 9a). Carbon uptake then declines over the remainder of the 21st century to $0.05\,Pg\,C\,yr^{-1}$ in 2100. This increased carbon uptake arising from forest harvesting reflects increased rates of biomass growth that occur following the removal of aboveground structural material from the ecosystems; however, it does not account for the loss of aboveground biomass into forest products and the subsequent carbon losses arising from their decay. When we consider the rate at which carbon is being stored within forests, the impact of forest harvesting is quite different (Fig. 9b). Before the 1920s, forest harvesting increases losses of stored carbon, increasing the peak loss rate to $0.67\,Pg\,C\,yr^{-1}$ in the late 1800s. Between 1920 and 1960, forest harvesting increases carbon storage due

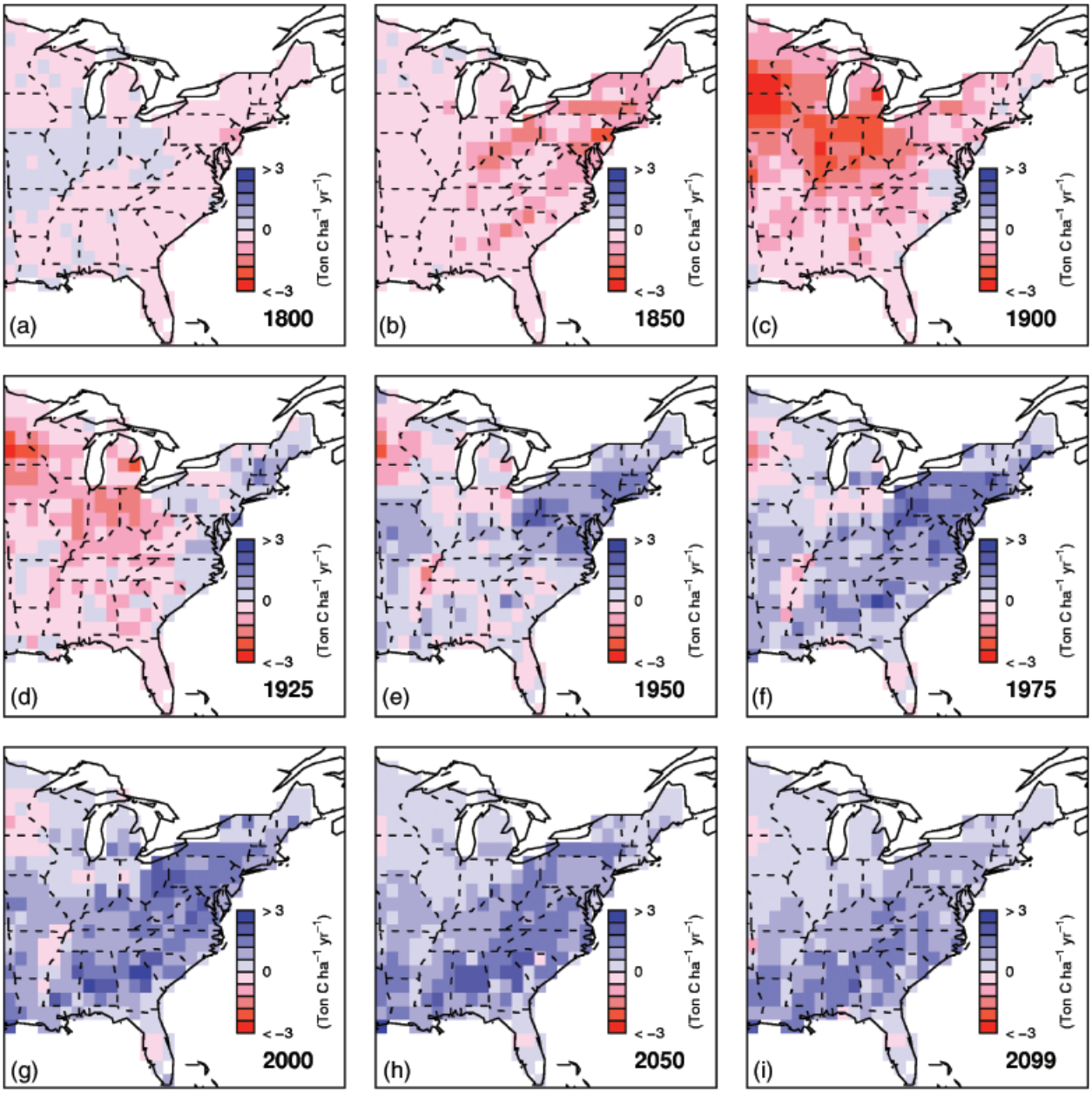

Fig. 8 Spatial patterns of annual rates of carbon uptake ($tC\,ha^{-1}\,yr^{-1}$) for selected years under the land-use change and forest-harvesting scenario (average of 3 years centered on each year shown). Positive values indicate a flux to the biosphere.

to a decline in harvesting rates during this period (see Fig. 3). After 1960, harvesting rates increase again, reducing the rate of carbon storage. The rate of carbon storage for the 1990s under the land-use change and forest harvesting scenario is 0.11, $0.03\,Pg\,C\,yr^{-1}$ less than under land-use change alone. During the 21st century, forest harvesting (Fig. 9b) reduces the rate of carbon storage to $0.01\,Pg\,C\,yr^{-1}$.

In addition to its effects on net carbon uptake, forest harvesting has a significant impact on forest composition and structure. For example, in central Massachusetts, recovery from agriculture in the absence of forest harvesting gives rise to forests comprised of a mixture of early successional deciduous, mid-successional deciduous and northern pines with a significant amount of the biomass found in large-sized trees (Fig. 10a). However, when forest harvesting is included, forest composition shifts towards a larger fraction of smaller sized, mid-successional deciduous trees (Fig. 10b) due to the increase in the fraction of secondary forests with lower mean ages (Fig. 10c and d).

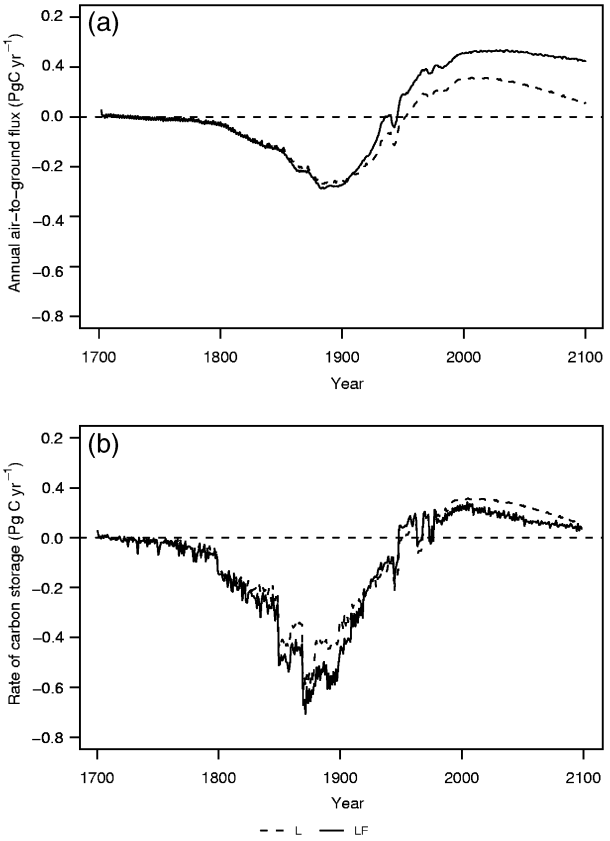

Fig. 9 Rates of (a) total carbon uptake (Pg C yr^{-1}), and (b) total carbon storage (Pg C yr^{-1}), arising from simulations for the region shown in Fig. 8, with land use only (L, dashed line) and land-use + forest harvesting (LF, solid line) history forcing. The high-frequency oscillations in the rate of carbon storage arise from the periodic nature of forest harvesting.

The addition of CO_2 fertilization into the model simulations has a significant impact on both rates of carbon uptake and carbon storage (Fig. 11). The rate of carbon uptake during the 1980s increases from 0.21 Pg C yr^{-1} in the absence of CO_2 fertilization to 0.39 Pg C yr^{-1} in the presence of CO_2 fertilization, and from 0.25 to 0.47 Pg C yr^{-1} in the 1990s. Similarly, the rate of carbon storage also increases from 0.10 to 0.25 Pg C yr^{-1} in the 1980s, and from 0.11 to 0.33 Pg C yr^{-1} in the 1990s (Fig. 11). The effects of CO_2 fertilization on carbon uptake then continues to increase throughout the 21st century, driven by the predicted rise of atmospheric CO_2 concentrations, with uptake rates of 0.76 Pg C yr^{-1} in the 2050s and 0.83 Pg C yr^{-1} by 2100 (Fig. 11).

Regional model-data comparison

The aboveground fraction of regional carbon uptake and storage predicted by the model simulations can be compared with measured rates of aboveground carbon uptake and storage from the USFSFIA program (Fig. 12). For the 1985–1996 period, which covers most of the state-wide census periods, the FIA observations indicate an average aboveground carbon uptake rate (biomass growth minus natural mortality) of 0.22 Pg yr^{-1}. Of this total, 0.09 Pg C yr^{-1} is stored in aboveground biomass (dashed lines in Fig. 12), and the remaining 0.13 Pg C yr^{-1} is lost as a result of forest harvesting. Comparison of the model results from the forest harvesting and land-use scenario (Fig. 12) predicts a total rate of aboveground uptake of 0.19 Pg C yr^{-1} for the 1985–1996 period, 0.03 Pg C yr^{-1} lower than the FIA estimate. As the figure shows, the difference is due to a lower rate of carbon storage, 0.06 Pg C yr^{-1}, as compared with the inventory estimate of 0.09 Pg C yr^{-1}. When CO_2 forcing is included in the model simulations, the predictions for carbon uptake increase to 0.28 Pg C yr^{-1} exceeding the observed uptake by 0.06 Pg C yr^{-1}. As the figure shows, this value arises as a result of increased biomass storage, 0.15 Pg C yr^{-1} as compared with the inventory estimate of 0.09 Pg C yr^{-1} (Fig. 12).

Site level model-data comparison

Figure 13 shows the predicted total NEP for the Harvard Forest grid-cell compared with the observed rate of net ecosystem exchange (NEE) measured at the Harvard Forest Eddy-covariance tower (Barford *et al*., 2001). Consistent with the earlier regional aboveground biomass growth comparison shown in Fig. 12, in the absence of CO_2 fertilization, the model underpredicts NEP by ~10% during these years (an average of 1.85 vs. 2.05 tC ha yr^{-1}), but the variability of predicted NEP is similar to that seen in NEE observations (solid line in Fig. 13a). During 1993 and 1994, the predicted NEP is substantially lower than the measured NEE; however, this corresponds to a large discrepancy between the NCEP precipitation data used in the model simulations, and the precipitation measured at the Harvard Forest weather station (see Fig. 13b). The addition of CO_2 fertilization into the model simulations results in a 28% over-prediction of NEP (an average of 2.64 vs. 2.05 tC ha yr^{-1} for the 1995–2000 period (dashed line in Fig. 13a).

Interannual climate variability

The incorporation of variable climate for the 1948–2003 period causes marked interannual variability in the net carbon fluxes from the region (Fig. 14a). Over the whole 1948–2003 period, the region is in positive carbon balance; however, the annual carbon fluxes fluctuate between a +0.5 Pg C yr^{-1} sink to a −0.6 Pg C yr^{-1} source

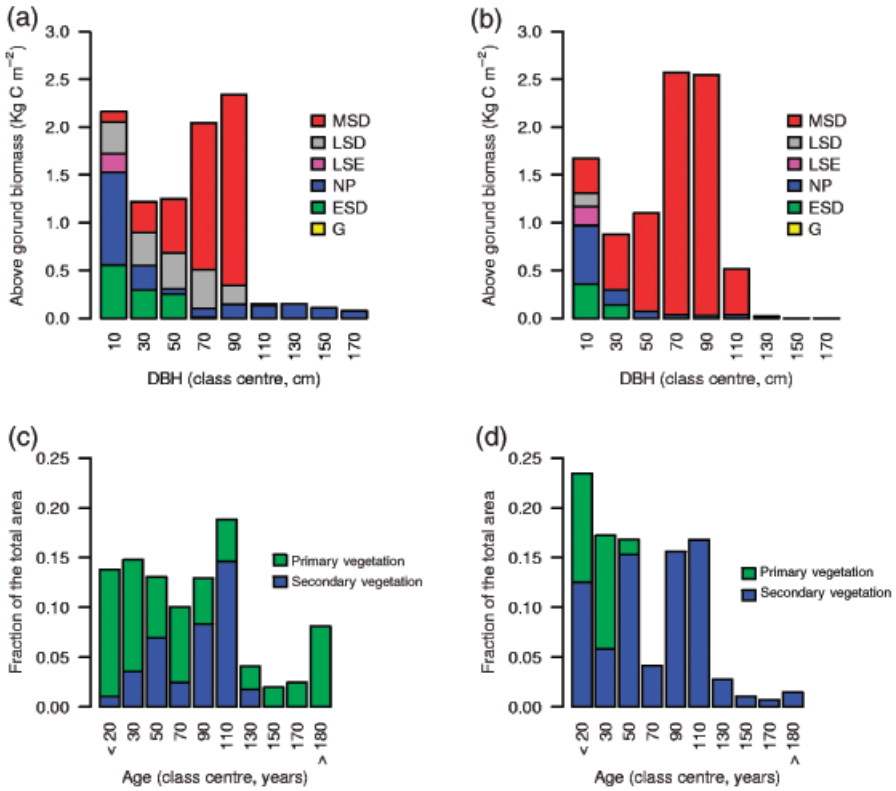

Fig. 10 Impact of land use and forest harvesting on forest composition in central Massachusetts for the year 2000. Panels a and b: Aboveground biomass (kg C m^{-2}) distribution by diameter size class and plant functional type. (a) land use only, (b) land use and forest harvesting. Panels (c) and (d): landscape age distribution of primary and secondary forests. (c) land use only, (d) land use and forest harvesting. Age is defined at the time since last disturbance in years.

(Fig. 14a). Carbon uptake rates are generally below average uptake during 1948–1980, generally above average in 1981–1998, and below average in 1999–2003 (Fig. 14a). Comparing the patterns of variability in NEP (Fig. 14a) with the patterns of temperature and precipitation variability (Fig. 4), reveals that the periods of carbon loss during the 1960s was caused by anomalously dry conditions, while the losses that occurred in the late 1990s were due to a combination of reduced precipitation and anomalously warm temperatures.

As Fig. 14b indicates, the influence of climate variability on the observed pattern of carbon fluxes is primarily the result of interannual variation in respiration rates, with warm and dry conditions causing significant increases in heterotrophic respiration rates. As most of the interannual variability in uptake arises from variation in heterotrophic respiration, climate variability has minimal impact on the decadal-scale patterns of aboveground carbon uptake and storage shown in Fig. 12. In the presence of inter-annual variability, the predicted rates of aboveground carbon uptake and carbon storage fluxes for the 1985–1996 period arising from forest harvesting and land-use scenario in climate are 0.19 and 0.06 Pg C yr^{-1}, respectively, values similar to those obtained under average climate.

Discussion

Our analysis incorporated the two dominant mechanisms hypothesized to be responsible for the current carbon sink in the Eastern United States: CO_2 fertilization and forest regrowth following agricultural abandonment and forest harvesting. In the absence of CO_2 enhancement, the simulations indicate carbon uptake of 0.21–0.25 Pg C yr^{-1} during the period 1980–2000. These rates are predicted to be maintained throughout the 21st century, but become increasingly dominated by forest regrowth: the predicted rate of actual carbon storage steadily declines from 0.11 Pg C yr^{-1} during the 1990s to under 0.01 Pg C yr^{-1} by 2100. Incorporation of CO_2 fertilization yields substantially increased rates of carbon uptake, contributing an additional 0.17–0.22 Pg C yr^{-1} during the period 1980–2000, and causing uptake to continue to rise during the 21st century, reaching 0.7 Pg C yr^{-1} by 2100. By this time, the effects of land-use recovery have ended, and

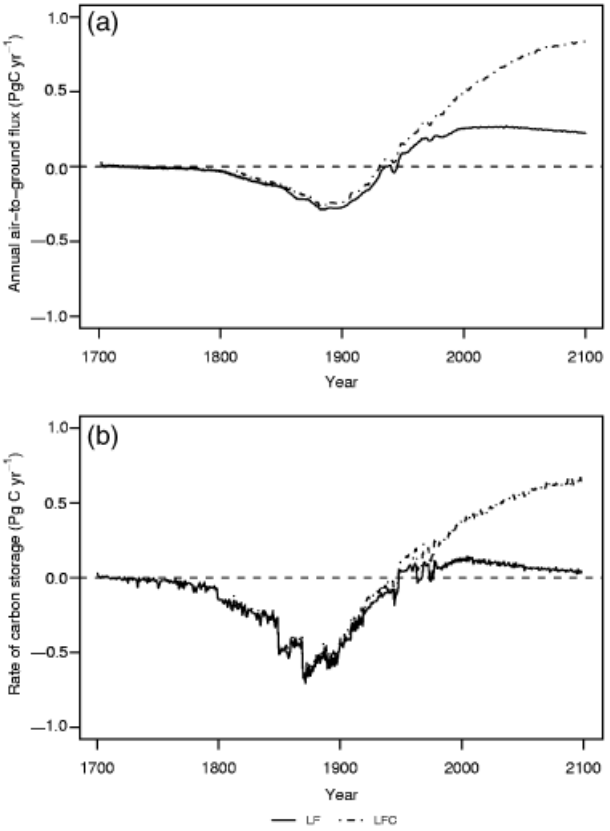

Fig. 11 Rates of (a) carbon uptake and (b) carbon storage after forcing the model with land use and forest harvesting (LF, solid line), and after forcing with CO_2 fertilization plus land use and forest harvesting (LFC, dot-dashed line). Units are Pg C yr^{-1}. The high-frequency oscillations in the rate of carbon storage arise from the periodic nature of forest harvesting in the model simulations.

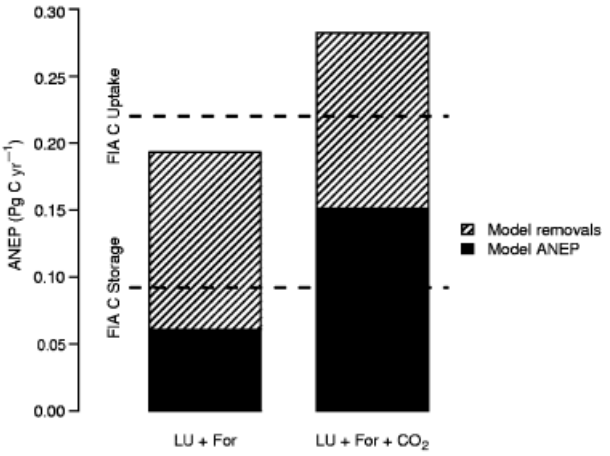

Fig. 12 Comparison of model results with forest inventory analysis-based estimates of carbon uptake and carbon storage in aboveground forest biomass (ANEP) in the average climate case. In the absence of CO_2 fertilization, the model under predicts the observed rates of carbon uptake and storage by 0.03 Pg C yr^{-1}, while in the presence of CO_2 fertilization, the model over-predicts the rates of uptake and storage by 0.06 Pg C yr^{-1}. Similar results are obtained with variable climate forcing.

CO_2 fertilization is responsible for the majority of carbon uptake, and virtually all carbon storage (Fig. 11b).

Comparison of the predicted aboveground carbon uptake rates to regional forest inventory data (Fig. 12) indicates that in the absence of CO_2 fertilization, the model simulations predict aboveground uptake rates 14% lower that the inventory measurements, but when CO_2 fertilization is added, the predicted uptake is 27% higher than is observed. A similar pattern is obtained in comparisons between the model's predictions of total NEP to observations at the Harvard Forest flux tower site (Fig. 13), with a 10% underestimation of the observed fluxes in the absence of CO_2 fertilization and 28% overprediction of NEP when CO_2 fertilization effects are included. The results of our regional and site-level comparisons thus suggest that while some degree of CO_2 fertilization may be occurring, terrestrial ecosystem models, including the ED model used in this study, require modification to take account of acclimatory responses to rising CO_2 levels.

Simulations of the model's predicted responses to CO_2 fertilization at three free-air CO_2 enrichment (FACE) sites located within the simulation domain further support this conclusion. Figure 15 shows the magnitude of the growth enhancement (relative increase in aboveground biomass accumulation in elevated CO_2 vs. ambient conditions) that occurs in ED model simulations of the Oak Ridge, Duke Forest, and Aspen FACE experiments. The initial magnitude of the growth enhancement predicted by the ED model simulations is either similar to (Aspen-FACE and Duke Forest), or below (Oak Ridge) the observed level of growth enhancement under elevated CO_2 conditions. However, in contrast to the observations, where the level of growth enhancement declines over time, the growth enhancement predicted by the ED model is either maintained (Aspen-FACE and Oak Ridge), or declines more slowly (Duke Forest) than is observed, implying that the model over-estimates the long-term rate of biomass accumulation arising from elevated levels of CO_2 (Fig. 15).

The increased growth in response to rising atmospheric CO_2 levels predicted by the ED model arises from the leaf physiology submodel developed by Farquhar, Collatz, Ball, Berry and others (see Appendix B sections for more details). Physiological studies at forest FACE sites indicate that leaf-level enhancement

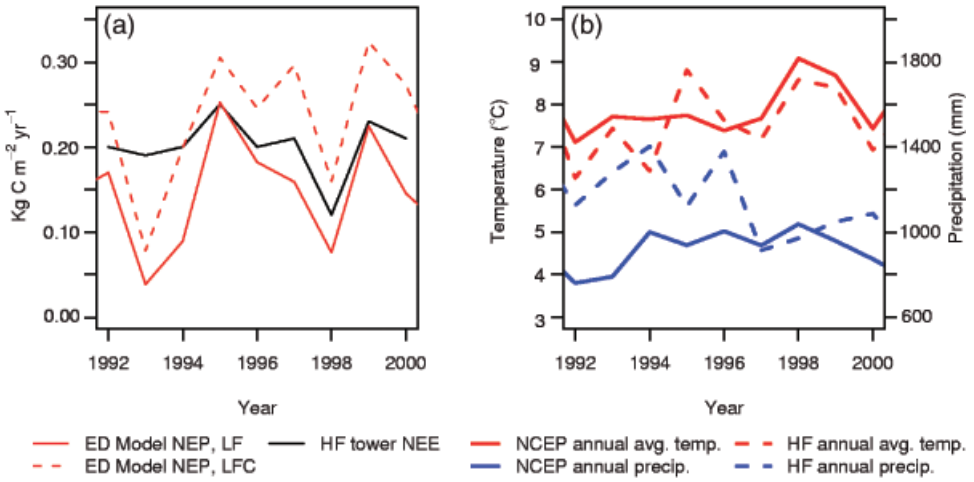

Fig. 13 (a) Comparison of the Harvard Forest eddy covariance measurements of net ecosystem exchange (NEE) with the ecosystem demography (ED) model simulation of annual net ecosystem productivity (NEP) for the grid cell of Harvard Forest under the land use and forest harvesting (LF), and the land use, forest harvesting, and CO_2 fertilization (LFC) scenarios. Units are kg C yr^{-1}. (b) Comparison of the NCEP temperature and precipitation data used in the regional model simulations with the observed meteorological data from the weather station at Harvard Forest.

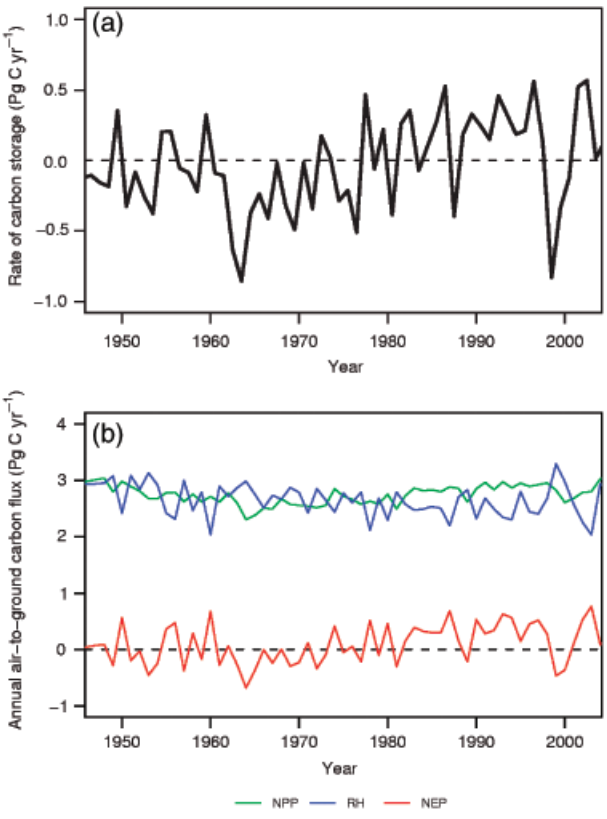

Fig. 14 (a) Rates of carbon uptake from the variable climate and land use and forest harvesting (LFC) simulation. Units are Pg C yr^{-1}. (b) Component fluxes for the simulation shown in (a) Net ecosystem productivity (NEP), net primary productivity (NPP), and heterotrophic respiration (RH) in Pg C yr^{-1}. Note that both NEP and RH exclude carbon fluxes to the atmosphere arising from the burning of slash and decomposition of forest products.

of photosynthesis does indeed occur (Blaschke *et al.*, 2001; Herrick & Thomas, 2001; Sholtis *et al.*, 2004; Korner *et al.*, 2005); however, it is accompanied by shifts in allocation away from structural pools toward short-lived, nonstructural carbon pools that do not significantly enhance the total aboveground biomass (Oren *et al.*, 2001; Norby *et al.*, 2002; Ellsworth *et al.*, 2004; Nowak *et al.*, 2004; Korner *et al.*, 2005; Finzi *et al.*, 2006; though see Hamilton *et al.*, 2002). In contrast, the patterns of allocation in the ED model are fixed, and thus the increased CO_2 uptake predicted by the Farquhar photosynthesis scheme directly translates into increased aboveground biomass accumulation. Additional studies at FACE sites indicate that the inferred shifts in patterns of plant carbon allocation occurring in response to elevated CO_2 are linked to nutrient limitation (Oren *et al.*, 2001; Norby *et al.*, 2002; Ellsworth *et al.*, 2004; Nowak *et al.*, 2004; Finzi *et al.*, 2006). As the results of this analysis indicate, there is an urgent need to develop more realistic biogeochemical formulations of plant growth, in which patterns of carbon allocation are linked to nutrient availability.

In assessing the robustness of these results, it is important to consider the extent to which the findings may be affected by inaccuracies in the disturbance history forcing applied in the model simulations. For example, overestimation of the extent of land clearance during the 1800s could conceivably result in an overestimate of the amount of regional uptake attributable to disturbance history. Conversely, if, in addition to the effects of land-use change and forest harvesting, the fire disturbance rates of forested lands in the East were also

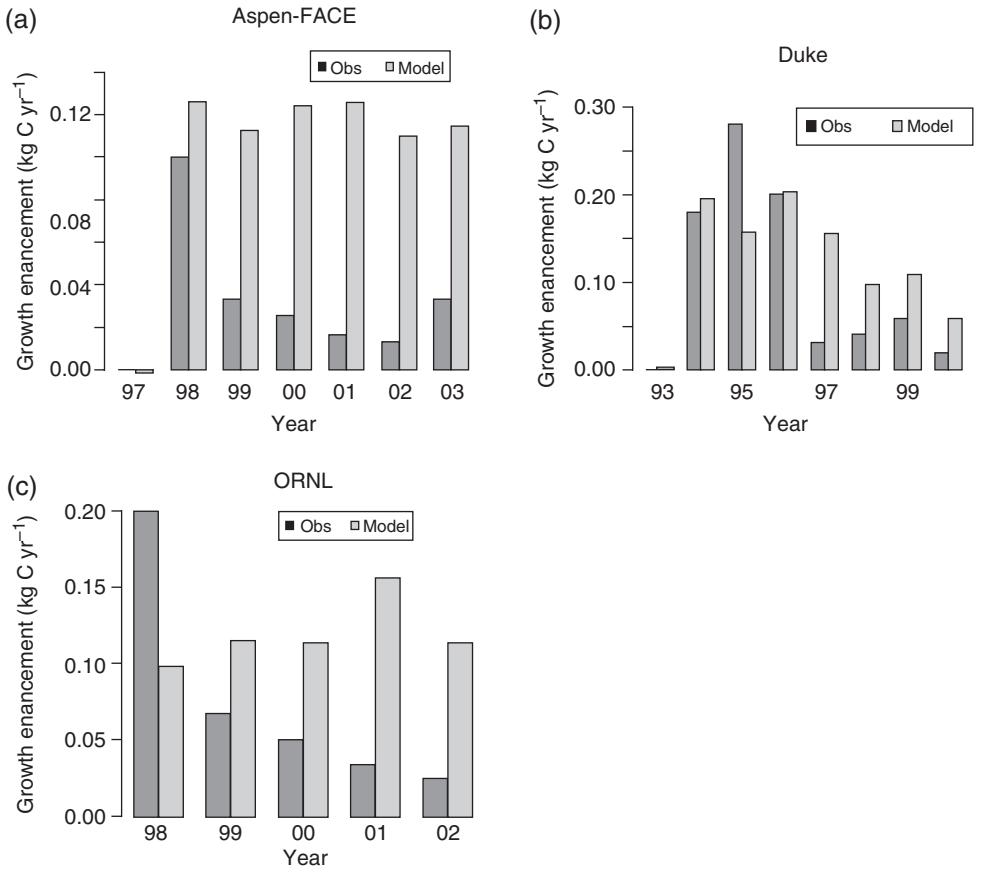

Fig. 15 Rates of growth enhancement predicted by the ecosystem demography (ED) model (gray bars) compared with observed rates of growth enhancement (black bars) in the (a) Oak ridge, (b) Aspen and (c) Duke forest free-air CO_2 enrichment (FACE) experiments. In the ED model simulations, the model was initialized with the observed stand structure and composition at the site and the CO_2 treatment was then applied. Onset years for elevated CO_2 treatments in the three experiments were 1998, 1998 and 1994, respectively. Bars indicate the difference in the magnitude of aboveground biomass accumulation between plots subject to elevated and ambient CO_2 levels. Units are $kg\,C\,m^2\,yr^{-1}$.

higher in the past, then the amount of regional carbon uptake attributable to disturbance history may have been under-estimated. However, compared with other areas of the globe, the history of United States land-cover change and forest harvesting is well known (Hurtt *et al.*, 2006) and fire suppression is thought to primarily contribute to carbon uptake in western forests (Pyne, 1982; Williams, 1989; Hurtt *et al.*, 2002; Houghton, 2003). Moreover, the above issues are unlikely to have affected the consistent results obtained from the comparison of NEP at Harvard Forest as the disturbance history of central Massachusetts is well documented and changes in fire suppression over the simulation period are unlikely to be an important factor in this region.

The magnitude of current carbon uptake attributable to land-use change and forest harvesting obtained from our model simulations is generally consistent with earlier estimates of the effects of disturbance history. Our estimate of the effects of land-use change and forest harvesting lies within Pacala *et al.*'s (2001) range of estimates for the forest carbon pools and wood products sink of $0.17–0.37\,Pg\,C\,yr^{-1}$. Houghton & Hackler (2000) and Hurtt *et al.* (2002) reported figures for the entire United States; however, most of the recovery from past land-use change in the United States occurred in the Eastern United States, the area considered in this study. We estimate a larger terrestrial carbon source during the late 1800s than Houghton & Hackler (2000) and Hurtt *et al.* (2002), who estimated peak losses of $\sim 0.4\,Pg\,C\,yr^{-1}$ for the entire coterminous United States, compared with our estimate of $\sim 0.67\,Pg\,C\,yr^{-1}$. For the post 1920 period, our simulations yield a larger land-use and forest harvesting sink than Houghton & Hackler (2000), $0.11\,Pg\,C\,yr^{-1}$ compared with $\sim 0.05\,Pg\,C\,yr^{-1}$. This difference is likely due to the differences in the effects of agriculture on soil carbon stocks. In Houghton & Hackler (2000), soil carbon losses upon conversion to agriculture are prescribed as 25% of the preexisting soil carbon, while in our simula-

tions the amount of soil carbon lost is determined by a process-based decomposition model that predicts substantially larger losses of soil carbon following agricultural conversion and thus a larger soil carbon sink during the recovery from past land-use. Excluding the effects of fire suppression that occur primarily in western regions, Hurtt *et al*. (2002) obtained carbon uptake rates arising from agricultural abandonment and forest harvesting sink $\sim 0.22\,\mathrm{Pg\,C\,yr^{-1}}$ for the 1980s, a value similar to the $0.21\,\mathrm{Pg\,yr^{-1}}$ obtained in this analysis.

In evaluating the contributions of the different processes to terrestrial carbon uptake, we considered two distinct carbon fluxes: net carbon uptake (sometimes referred to as 'apparent uptake') and actual carbon storage. The actual amount of carbon accumulation occurring at a given time will fall somewhere between these two measures. The extent to which forest products contribute to storage is complex, depending on harvesting technique and efficiency, the type of wood products produced, and their lifetimes. The time-scale at which wood products re-enter the atmosphere is highly variable, with estimates of product half-life ranging from 1 year for paper to 100 years for construction wood (Skog & Nicholson, 2000). In addition, global trade in forest products and their derivates influences the regional accounting of carbon storage in forest products (Nabuurs & Sikkema, 2001).

Another significant finding of this study is the significant impact of interannual climate variability on regional carbon uptake rates (Fig. 13). Specifically, the relatively dry period in the 1960s and the exceptionally warm years in the late 1990s are correlated with significant reductions in carbon uptake and storage (Fig. 4), with this interannual variability being driven primarily by changes in heterotrophic respiration. The area considered in this study is smaller than the typical subregions considered in atmospheric inversions; however, the existence of significant long-term carbon uptake in the Eastern United States is consistent with the findings of recent inversion studies (Rodenbeck *et al*., 2003; Peylin *et al*., 2005; Baker *et al*., 2006).

With regard to patterns of interannual variability, the model's prediction of sustained uptake during the early 1990s was caused in part by the effects of above-average precipitation on plant growth, but primarily thorough a reduction in the rate of soil carbon decomposition due to below-average temperatures (Rodenbeck *et al*., 2003; Baker *et al*., 2006; Peylin *et al*., 2005). These results thus reaffirm the importance of incorporating interannual climate-variability into simulations of the terrestrial carbon cycle, and the need for long-term observations of ecosystem fluxes in order to reliably estimate the magnitude of average long-term uptake (Goulden *et al*., 1996; Potter *et al*., 1999; Goetz, 2000; Barford *et al*., 2001).

Acknowledgments

P. R. Moorcroft gratefully acknowledges funding from the Harvard University William F. Milton Fund; the Harvard Forest LTER; the Harvard University Center for the Environment; the Office of Science, Biological and Environmental Research Program (BER), US Department of Energy, through the Northeast Regional Center) of the National Institute for Global Environmental Change (NIGEC) under Cooperative Agreement No. DE-FC02-03ER63613; and National Science Foundation BE/CBC program Grant ATM-0221850. G. C. Hurtt gratefully acknowledges the support of the NASA Interdisciplinary Science Program. NCEP Reanalysis data was provided by the NOAA-CIRES Climate Diagnostics Center, Boulder, Colorado, USA (http://www.cdc.noaa.gov/). Thanks to D. Lipsitt for assistance with the model simulations.

References

Baker DF, Law RM, Gurney KR *et al*. (2006) TransCom 3 inversion intercomparison: impact of transport model errors on the interannual variability of regional CO_2 fluxes, 1988–2003. *Global Biogeochemical Cycles*, **20**, 1–17.

Ball JT, Woodrow IE, Berry JE (1986) *A model predicting stomatal conductance and its contribution to the control of photosynthesis under different environmental conditions*, Vol. 4. Martinus-Nijhoff\Springer-Verlag, Dordrecht, the Netherlands\New York, USA.

Barford CC, Wofsy SC, Goulden ML *et al*. (2001) Factors controlling long and short-term sequestration of atmospheric CO_2 in a mid-latitude forest. *Science*, **294**, 1688–1691.

Bauer GA, Berntson GM, Bazzaz FA (2001) The effect of elevated CO_2 and increased N availability on regenerating temperate forest communities: biochemical versus stomatal limitation of photosynthesis. *New Phytologist*, **152**, 249–266.

Birdsey RA, Heath LS (1995) Carbon changes in US forests. In: *Productivity of America's Forest and Climatic Change. US Department of Agriculture, Forest Service General Technical Report RM-271* (ed. Joyce LA), pp. 56–70. US Department of Agriculture, Forest Service, Washington, DC.

Blaschke LM, Schulte M, Raschi A *et al*. (2001) Photosynthesis, soluble and structural carbon compounds in two Mediterranean oak species (*Quercus pubescens* and *Q. ilex*) after lifetime growth at naturally elevated CO_2 concentrations. *Plant Biology*, **3**, 288–297.

Botta A, Viovy N, Ciais P *et al*. (2000) A global prognostic scheme of leaf onset using satellite data. *Global Change Biology*, **6**, 709–726.

Brown SP, Schroeder P, Birdsey R (1997) Aboveground biomass distribution of US eastern hardwood forests and the use of large trees as an indicator of forest development. *Forest Ecology and Management*, **96**, 37–47.

Burns RM, Honkala BH (1990a) *Silvics of North America: 1 Conifers. Agriculture Handbook 654*, Vol. 1. US Department of Agriculture, Forest Service, Washington, DC.

Burns RM, Honkala BH (1990b) *Silvics of North America: 2 Hardwoods. Agriculture Handbook 654*, Vol. 2. US Department of Agriculture, Forest Service, Washington, DC.

Cao M, Woodward FI (1998) Dynamic responses of terrestrial ecosystem carbon cycling to global climate change. *Nature*, **393**, 249–252.

Caspersen J, Pacala S, Jenkins J *et al*. (2000) Contributions of land-use history and enhanced tree growth to carbon accumulation in US forests. *Science*, **290**, 1148–1151.

Catovsky S, Bazzaz FA (2000) Contributions of coniferous and broad-leaved species to temperate forest carbon uptake: a bottom-up approach. *Canadian Journal of Forest Research*, **30**, 100–111.

Catovsky S, Holbrook NM, Bazzaz FA (2002) Coupling whole-tree transpiration and canopy photosynthesis in coniferous and broad-leaved tree species. *Canadian Journal of Forest Research*, **32**, 295–309.

Collatz GJ, Ball JT, Grivet C *et al*. (1991) Physiological and environmental regulation of stomatal conductance, photosynthesis and transpiration: a model that includes a laminar boundary layer. *Agricultural and Forest Meteorology*, **54**, 107–136.

Collatz GJ, Ribas-Carbo M, Berry JA (1992) Coupled photosynthesis-stomatal conductance model for leaves of C_4 plants. *Australian Journal of Plant Physiology*, **19**, 519–538.

Donnelly D, Lilly B, Smith E (2001) The Southern Variant of the Forest Vegetation Simulator. Fort Collins, CO: US Department of Agriculture, Forest service, Forest Management Service Center.

Ellsworth DS, Reich PB, Naumburg ES *et al*. (2004) Photosynthesis, carboxylation and leaf nitrogen responses of 16 species to elevated pCO_2 across four free-air CO_2 enrichment experiments in forest, grassland and desert. *Global Change Biology*, **10**, 1–18.

FAO (2004) FAOSTAT. Forestry Data. http://www.fao.org/forestry

Farquhar GD, Sharkey TD (1982) Stomatal conductance and photosynthesis. *Annual Review of Plant Physiology*, **33**, 317–345.

Farquhar GD, Von Caemmerer S, Berry JA (1980) A biochemical model of photosynthetic CO_2 assimilation in leaves of C_3 species. *Planta*, **149**, 78–90.

Finzi AC, Moore DJP, DeLucia EH *et al*. (2006) Progressive nitrogen limitation of ecosystem processes under elevated CO_2 in a warm-temperate forest. *Ecology*, **87**, 15–25.

Goetz SJ (2000) Interannual variability of global terrestrial primary production: results of a model driven with satellite observations. *Journal of Geophysical Research*, **105**, 20077–20092.

Goodale CL, Apps MJ, Birdsey RA *et al*. (2002) Forest carbon sinks in the Northern Hemisphere. *Ecological Applications*, **12**, 891–899.

Goulden ML, Munger JW, Fan SM *et al*. (1996) Exchange of carbon dioxide by a deciduous forest: response to interannual climate variability. *Science*, **271**, 1576–1578.

Hair D (1958) *Historical Forestry Statistics of the United States. Statistical Bulletin 228* US Department of Agriculture, Forest Service Washington, DC.

Hamilton JG, Delucia EH, George R *et al*. (2002) Forest carbon balance under elevated CO_2. *Oecologia*, **131**, 250–260.

Haynes RW (2003) An analysis of the timber situation in the United States: 1952 to 2050. *General Technical Report PNW-GTR-560*. US Department of Agriculture, Forest Service, Pacific Northwest Research Station, Portland, OR, 254 pp.

Herrick JD, Thomas RB (2001) No photosynthetic down-regulation in sweetgum trees (*Liquidambar styraciflua* L.) after three years of CO_2 enrichment at the Duke Forest FACE experiment. *Plant, Cell and Environment*, **24**, 53–64.

Houghton RA (2003) Why are estimates of the terrestrial carbon balance so different? *Global Change Biology*, **9**, 500–509.

Houghton RA, Hackler JL (2000) Changes in terrestrial carbon storage in the United States 1: the roles of agriculture and forestry. *Global Ecology and Biogeography*, **9**, 125–144.

Houghton RA, Hackler JL, Lawrence KT (1999) The US carbon budget: contributions from land-use change. *Science*, **285**, 574–578.

Hurtt GC, Frokling S, Feardon MG *et al*. (2006) The underpinnings of land-use history: three centuries of 4 global gridded transitions, wood harvest activity and resulting secondary lands. *Global Change Biology*, **12**, 1208–1229.

Hurtt GC, Moorcroft PR, Pacala SW *et al*. (1998) Terrestrial models and global change: challenges for the future. *Global Change Biology*, **4**, 581–590.

Hurtt GC, Pacala SW, Moorcroft PR *et al*. (2002) Projecting the future of the US Carbon sink. *Proceedings of the National Academy of Sciences*, **99**, 1389–1394.

IPCC (1998) *An introduction to simple climate models used in the IPCC second assessment report. IPCC Technical Paper II,* WMO/UNEP, Geneva, 47 pp.

Jain AK, Yang X (2005) Modeling the effects of two different land cover change data sets on the carbon stocks of plants and soils in concert with CO_2 and climate change. *Global Biogeochemical Cycles*, **19**, 1–20.

Joos F, Prentice IC, House JI (2002) Growth enhancement due to global atmospheric change as predicted by terrestrial ecosystem models: consistent with US forest inventory data. *Global Change Biology*, **8**, 299–303.

Joos F, Prentice IC, Sitch S *et al*. (2001) Global warming feedbacks on terrestrial carbon uptake under the Intergovermental Panel on Climate Change (IPCC) emission scenarios. *Global Biogeochemical Cycles*, **15**, 891–907.

Kalnay E, Kanamitsu M, Kistler R *et al*. (1996) The NCEP/NCAR 40-year reanalysis project. *Bulletin of American Meteorological Society*, **77**, 437–471.

Kicklighter DW, Bruno M, Dönges S *et al*. (1999) A first-order analysis of the potential role of CO_2 fertilization to affect the global carbon budget: a comparison study of four terrestrial biosphere models. *Tellus*, **51B**, 343–366.

Kistler R, Kalnay E, Collins W *et al*. (2001) The NCEP/NCAR 50-year reanalysis: monthly means CD-ROM and documentation. *Bulletin of American Meteorological Society*, **82**, 247–281.

Kittel TGF, Royle JA, Daly C *et al*. (1997) A gridded historical (1895–1993) bioclimate dataset for the conterminous United States. In: *Proceedings of the 10th Conference on Applied Climatology, 20–24 October 1997, Reno, NV* pp. 219–222. American Meteorological Society, Boston.

Korner C, Asshoff R, Bignucolo O *et al*. (2005) Carbon flux and growth in mature deciduous forest trees exposed to elevated CO_2. *Science*, **309**, 1360–1362.

Leuning R (1995) A critical appraisal of a combined stomatal-photosynthesis model for C_3 plants. *Plant, Cell and Environment*, **18**, 339–355.

McGuire AD, Sitch S, Clein JS *et al*. (2001) Carbon balance of the terrestrial biosphere in the twentieth century: analyses of CO_2, climate and land use effects with four process-based ecosystem models. *Global Biogeochemical Cycles*, **15**, 183–206.

Moorcroft PR (2003) Recent advances in ecosystem-atmosphere interactions: an ecological perspective. *Proceedings of the Royal Society Series B*, **270**, 1215–1227.

Moorcroft PR, Hurtt GC, Pacala SW (2001) A method for scaling vegetation dynamics: the ecosystem demography model (ED). *Ecological Monographs*, **74**, 557–586.

Nabuurs GJ, Schelhaas M-J, Mohren GMJ *et al*. (2003) Temporal evolution of the European forest sector carbon sink from 1950 to 1999. *Global Change Biology*, **9**, 152–160.

Nabuurs GJ, Sikkema R (2001) International trade in wood products: its role in the land use change and forestry carbon cycle. *Climatic Change*, **49**, 377–395.

Nobel IR, Slayter RO (1980) The use of vital attributes to predict successional changes plant communities subject to recurrent disturbance. *Vegetation*, **43**, 5–21.

Norby RA, Hanson PJ, O'Neill EG *et al*. (2002) Net Primary Productivity of a CO_2-enriched deciduous forest and the implications for carbon storage. *Ecological Applications*, **12**, 1261–1266.

Nowak RS, Smith SD, Ellsworth DS (2004) Functional responses of plants to elevated atmospheric CO_2 – do photosynthetic and productivity data from FACE experiments support early predictions? *New Phytologist*, **162**, 253–280.

Oren R, Ellsworth DS, Johnsen KH *et al*. (2001) Soil fertility limits carbon sequestration by forest ecosystems in a CO_2-enriched atmosphere. *Nature*, **411**, 469–473.

Pacala SW, Canham CD, Saponara J *et al*. (1996) Forest models defined by field measurements: estimation, error analysis and dynamics. *Ecological Monographs*, **66**, 1–43.

Pacala SW, Caspersen J, Hansen M (2004) Forest inventory data falsify ecosystem models of CO_2 fertilization. ESA Annual Meeting, Portland OR, August 1–9 2004.

Pacala SW, Hurtt GC, Baker D *et al*. (2001) Consistent land-and atmosphere-based US carbon sink estimates. *Science*, **292**, 2316–2320.

Parton WJ, Schimel DS, Cole CV *et al*. (1987) Analysis of factors controlling soil organic matter levels in Great Plains grasslands. *Soil Science Society of America Journal*, **51**, 1173–1179.

Peng CH (1999) *Non-linear height-diameter models for nine boreal forest tree species in Ontario*. Ministry of Natural Resources, Ontario Forest Research Institute, OFRI-Report 155, 28 pp.

Peylin P, Bousquet P, LeQuere C *et al*. (2005) Multiple constraints on regional CO_2 flux variations over land and oceans. *Global Biogeochemical Cycles*, **19**, GB1011, doi: 10.1029/2003GB002214.

Potter CS, Klooster S, Brooks V (1999) Interannual variability in Terrestrial Net Primary Production: exploration of trends and controls on regional to global scales. *Ecosystems*, **2**, 36–48.

Pyne SJ (1982) *Fire in America*. Princeton University Press, Princeton, NJ.

Ramankutty N, Foley JA (1999) Estimating historical changes in global land cover: croplands from 1700 to 1992. *Global Biogeochemical Cycles*, **13**, 997–1027.

Reich PB, Walters MB, Ellsworth DS (1997) From tropics to tundra: global convergence in plant functioning. *Proceedings of the National Academy of Sciences USA*, **94**, 13730–13734.

Reich PB, Walters MB, Ellsworth DS *et al*. (1998a) Relationships of leaf dark respiration to leaf nitrogen, specific leaf area and leaf life-span: a test across biomes and functional groups. *Oecologia*, **114**, 471–482.

Reich PB, Walters MB, Tjoelker MG *et al*. (1998b) Photosynthesis and respiration rates depend on leaf and root morphology and nitrogen concentration in nine boreal tree species differing in relative growth rate. *Functional Ecology*, **12**, 406–412.

Reynolds RV, Pierson AH (1942) *Fuelwood Used in the Unites States 1630–1930. Circular 641*. US Department of Agriculture, Washington, DC.

Rodenbeck CS, Houweling S, Gloor M *et al*. (2003) CO_2 flux history 1982–2001 inferred from atmospheric data using a global inversion of atmospheric transport. *Atmospheric Chemistry and Physics Discussions*, **3**, 2575–2659.

Saki Weiser (1973) Freezing resistance of trees in North America with reference to tree regions. *Ecology*, **54**, 118–126.

Schimel DS (1995) Terrestrial ecosystems and the carbon cycle. *Global Change Biology*, **1**, 77–91.

Schimel DS, House JI, Hibbard KA (2001) Recent patterns and mechanisms of carbon exchange by terrestrial ecosystems. *Nature*, **414**, 169–172.

Schimel D, Melillo J, Tian H (2000) Contributions of increasing CO_2 and climate to carbon storage by ecosystems in the United States. *Science*, **287**, 2004–2006.

Sholtis JD *et al*. (2004) Persistent stimulation of photosynthesis by elevated CO_2 in a sweetgum (*Liquidambar styraciflua*) forest stand. *New Phytologist*, **162**, 343–354.

Skog KE, Nicholson GA (2000) Carbon sequestration in wood and paper products. In: *The Impact of Climate Change on America's Forests: A Technical Document Supporting the 2000 USDA Forest Service RPA Assessment, General Technical Report RMRS-GTR-59* (eds Joyce LA, Birdsey R), pp. 79–88. US Department of Agriculture, Forest Service, Rocky Mountain Research Station, Fort Collins, CO.

Ter-Mikaelian MT, Korzukhin MD (1997) Biomass equations for sixty-five North American tree species. *Forest Ecology and Management*, **97**, 1–24.

US Bureau of the Census (1997) *Historical Statistics of the United States on CD-ROM: Colonial Times to 1970*. Cambridge University Press, New York.

Villar R, Merino J (2001) Comparison of leaf construction costs in woody species with differing leaf life-spans in contrasting ecosystems. *New Phytologist*, **151**, 213–226.

Waisanen PJ, Bliss NB (2002) Changes in population and agricultural land in conterminous United States counties, 1790 to 1997. *Global Biogeochemical Cycles*, **16**, 1137–1138.

White MA, Thornton PE, Running SW (1997) A continental phenology model for monitoring vegetation responses to interannual climatic variability. *Global Biogeochemical Cycles*, **11**, 217–234.

Williams M (1989) *Americans and Their Forests: A Historical Geography*. Cambridge University Press, Cambridge.

Wullschleger SD (1993) Biochemical limitations to carbon assimilation in C_3 plants – A retrospective analysis of the A/C_i curves from 109 species. *Journal of Experimental Botany*, **44**, 907–920.

Appendix A: dynamics of belowground decomposition

The decomposition submodel used in the model simulations was the same as Moorcroft *et al*. (2001), consisting of five pools: a fast carbon pool (C_1), a slow carbon pool (C_2), associated fast (N_1) and slow (N_2) nitrogen pools, and a pool of mineralized nitrogen (N) available for plant uptake. Carbon and nitrogen flow into the belowground pools from the aboveground pools as the consequence of two processes: tissue decay and mortality of plants. $C^{(i)}_{a,\mathrm{dead}}(\mathbf{z},a,t)$ and $C^{(i)}_{s,\mathrm{dead}}(\mathbf{z},a,t)$ are the fluxes of carbon into the fast and slow carbon pools due to the death of individuals of type i, size $\mathbf{z}$ in places within the grid cell disturbed a years ago, and $N^{(i)}_{a,\mathrm{dead}}$ and $N^{(i)}_{s,\mathrm{dead}}$ are the corresponding nitrogen inputs into the fast and slow nitrogen pools. These fluxes are given by:

$$\begin{aligned} C^{(i)}_{a,\mathrm{dead}} &= \mu(\mathbf{z},\mathbf{r},t)C_a(\mathbf{z},a,t),\\ C^{(i)}_{s,\mathrm{dead}} &= \mu(\mathbf{z},\mathbf{r},t)C_s(\mathbf{z},a,t),\\ N^{(i)}_{a,\mathrm{dead}} &= \mu(\mathbf{z},\mathbf{r},t)C_a(\mathbf{z},a,t)/(\mathrm{C:N})_a,\\ N^{(i)}_{s,\mathrm{dead}} &= \mu(\mathbf{z},\mathbf{r},t)C_s(\mathbf{z},a,t)/(\mathrm{C:N})_s. \end{aligned} \tag{A1}$$

where $\mu(\mathbf{z},\mathbf{r},t)$ is the mortality rate of individuals of type i, size $\mathbf{z}$ experiencing resource conditions $\mathbf{r}$; C_a and C_s are, respectively, the living and structural biomass density of individuals of type i size $\mathbf{z}$ in places disturbed a years ago; and $(\mathrm{C:N})_a$ and $(\mathrm{C:N})_s$ are the carbon to nitrogen ratio in living and structural biomass tissues.

The decomposition rates of the fast and the slow pools, respectively $C_{1,\mathrm{decomp}}(a,t)$ and $C_{2,\mathrm{decomp}}(a,t)$, have intrinsically different decay times, and are modified by a common function $A(a,t)$ taken directly from the CENTURY model that varies between 0 and 1 depending on soil temperature, moisture and texture, and potential evapotranspiration (see Parton *et al*., 1987):

$$\begin{aligned} C_{1,\mathrm{decomp}}(a,t) &= 11.0A(a,t)\,C_1(a,t),\\ C_{2,\mathrm{decomp}}(a,t) &= 0.22A(a,t)\,C_2(a,t)\,c^*_{im}. \end{aligned} \tag{A2}$$

Soil temperature values are specified from the NCEP/NCAR Reanalysis 1 forcing dataset while soil moisture availability is modeled using a simple single layer soil hydrology model (see Moorcroft *et al*., 2001 Appendices G and H for further details).

The nitrogen mineralization rates $N_{1,\mathrm{min}}(a,t)$ and $N_{2,\mathrm{min}}(a,t)$ are directly proportional to the carbon decomposition rates:

$$\begin{aligned} N_{1,\mathrm{min}}(a,t) &= 11.0A(a,t)N_1(a,t),\\ N_{2,\mathrm{min}}(a,t) &= 0.22A(a,t)N_2(a,t)c^*_{im}. \end{aligned} \tag{A3}$$

The term c^*_{im} in Eqns (A2) and (A3) is a (0–1) function of the immobilization demand for nitrogen relative to the supply $(D:S)_{im}$, so that decomposition and nitrogen mineralization of high C:N structural material are halted if mineralized nitrogen availability is low:

$$c^*_{im} = \frac{1}{1+(D\,:\,S)_{im}}, \tag{A4}$$

where $D = 0.22\,A(a,t)\,C_2 \times 0.65$ is calculated as the nitrogen necessary for a reduction in the C:N ratio of the structural material from 150 to 10, assuming a respiration of 30% (Parton *et al*., 1987). The supply of nitrogen $S = vN$ is assumed to be proportional to the mineralized nitrogen pool N, with $v = 40$ set to a high value relative to that of plants, under the assumption that microbes have greater access to available nitrogen than plants.

The system of belowground equations for carbon and nitrogen is:

$$\begin{aligned} \frac{\mathrm{d}C_1(a,t)}{\mathrm{d}t} &= \sum_i \int_{z_0}^{\infty} C_{\mathrm{litter}}(\mathbf{z},\mathbf{r},a,t)\,\mathrm{d}z\\ &\quad + \sum_i \int_{z_0}^{\infty} C_{a,\mathrm{dead}}(\mathbf{z},\mathbf{r},a,t)\,\mathrm{d}z - C_{1,\mathrm{decomp}}(a,t),\\ \frac{\mathrm{d}C_2(a,t)}{\mathrm{d}t} &= \sum_i \int_{z_0}^{\infty} C_{s,\mathrm{dead}}(\mathbf{z},\mathbf{r},a,t)\,\mathrm{d}z - C_{2,\mathrm{decomp}}(a,t), \end{aligned} \tag{A5}$$

$$\begin{aligned} \frac{\mathrm{d}N_1(a,t)}{\mathrm{d}t} &= \sum_i \int_{z_0}^{\infty} N_{\mathrm{litter}}(\mathbf{z},\mathbf{r},a,t)\,\mathrm{d}z\\ &\quad + \sum_i \int_{z_0}^{\infty} N_{a,\mathrm{dead}}(\mathbf{z},\mathbf{r},a,t)\,\mathrm{d}z - N_{1,\mathrm{min}}(a,t),\\ \frac{\mathrm{d}N_2(a,t)}{\mathrm{d}t} &= \sum_i \int_{z_0}^{\infty} N_{s,\mathrm{dead}}\ (\mathbf{z},\mathbf{r},a,t)\,\mathrm{d}z - N_{2,\mathrm{min}}(a,t),\\ \frac{\mathrm{d}N(a,t)}{\mathrm{d}t} &= N_{1,\mathrm{min}}(a,t) + N_{2,\mathrm{min}}(a,t)\\ &\quad - \sum_i \int_{z_0}^{\infty} c_i(\mathbf{z},a,t)N_{\mathrm{up}}(\mathbf{z},\mathbf{r},a,t)\,\mathrm{d}z. \end{aligned} \tag{A6}$$

where variables C_{litter} and N_{litter} are the carbon and nitrogen lost by individuals due to tissue decay and leaf drop (see Moorcroft *et al*., 2001), N_{up} is the nitrogen uptake from the plant community, and the other variables and functions have been described earlier.

Appendix B: parameterization of PFTs

Leaf physiology

The physiology submodel of ED model uses the schemes developed by Farquhar & Sharkey (1982); Ball *et al*. (1986); Collatz *et al*. (1991, 1992) and Leuning

(1995) for predicting carbon fixation and evapotranspiration per unit leaf area from standard climatological inputs (see Moorcroft *et al*., 2001, Appendix A). The seven PFTs in this study were assigned different values of Vm_0 that reflecting differences in their maximum rate of photosynthesis per unit leaf area and light compensation point (Wullschleger, 1993; Reich *et al*., 1998b; Catovsky & Bazzaz, 2000; Catovsky *et al*., 2002) and shade tolerance (Burns & Honkala, 1990a, b). Early successional hardwoods have a Vm_0 of $18.25\,\mu mol\,m^{-2}\,s^{-1}$, early successional conifers and mid-successional hardwoods had a Vm_0 of $15.626\,\mu mol\,m^{-2}\,s^{-1}$, while late successional conifers and late successional hardwoods have a Vm_0 of $6.25\,\mu mol\,m^{-2}\,s^{-1}$ (Table 1). A second important leaf physiology characteristic represented in ED is differences in specific leaf area (SLA), which controls the leaf area return of the plant's investment in leaf biomass, and consequently the rate of GPP per unit leaf biomass. For a given Vm_0, high SLA PFTs have a higher rate of GPP per unit leaf biomass than low SLA PFTs. SLA values were assigned based on species-specific values from Reich *et al*. (1998a), Villar & Merino (2001), Bauer *et al*. (2001) and from values measured at Harvard Forest (J. Hadley, personal communication) (see Table 1). Leaf foliar nitrogen content for each PFT is then determined from the PFT's Vm_0 and SLA values using the linear relationship between night-time respiration and Vm_0, and the observed relationship between per unit area foliar nitrogen content and night-time respiration (Reich *et al*., 1998a, b).

Leaf longevity

In a manner identical to the drought-deciduous phenology scheme described in Moorcroft *et al*. (2001), cold-deciduous PFTs lose 50% of their leaf biomass when leaf drop occurs (see *'Phenology'*). Leaf longevities of the coniferous PFTs were specified as 3 years, a value consistent with the empirical SLA-leaf longevity relationship measured by Reich *et al*. (1997).

Allometry and allocation

The height–diameter relationships for the PFTs were specified from Pacala *et al*. (1996)

$$H = 1.3 + b_{1h}(1 - e^{b_{2h}\mathrm{DBH}}), \tag{B1}$$

where H is the tree's height in meters, DBH its diameter at breast height in centimeters. Estimates for b_{1h} and b_{2h} for each PFT were obtained by fitting Eqn (B1) to published height-DBH relationships of canonical species (Peng, 1999; Donnelly *et al*., 2001). Equations similar to those used in Moorcroft *et al*. (2001), were used to describe the relationships between DBH and structural biomass (B_s), and DBH between and foliar biomass (B_l):

$$B_s = a_s \mathrm{DBH}^{b_s}, \tag{B2}$$

$$B_l = \begin{cases} a_l \mathrm{DBH}^{b_l} & \text{if } (\mathrm{DBH} \le \mathrm{DBH}_{max}) \\ a_l \mathrm{DBH}_{max}^{b_l} & \text{if } (\mathrm{DBH} > \mathrm{DBH}_{max}). \end{cases} \tag{B3}$$

The values of a_l, b_l, a_s and b_s in Eqns (B2) and (B3) were calculated for each PFT from representative species-specific allometric equations (Ter-Mikaelian & Korzukhin (1997) – see Table 2.

As in the original ED formulation, the above empirical allometric curves are used in conjunction with the prescribed rates of tissue turnover for each PFT to determine the size-specific pattern of carbon and nitrogen allocation between the different biomass compartments (see Moorcroft *et al*., 2001, Appendices D and E).

Phenology

The drought-deciduous phenology scheme used in the ED implementation for South America (Moorcroft *et al*., 2001) was replaced by Botta *et al*.'s (2000) cold-deciduous phenology scheme, in which leaf onset occurs when the thermal sum of growing degree-days exceeds a threshold determined by an exponential function of the number of chill days. Leaf offset is determined by photoperiod and soil temperature: leaves drop when the day length is less than 655 min and monthly average air temperature is less than 11.15 °C, or when monthly average air temperature is less than 2.0 °C independently of photoperiod (White *et al*., 1997). In the original model fitting of White *et al*. (1997), the temperature trigger was an 11-day running average of the daily mean temperature. Average temperatures, day lengths, and thermal sums are computed for each month.

Mortality

Density independent mortality rates for each PFT were obtained from the USFIA data for trees above 10 cm in diameter. Differences in the tolerance of the PFTs minimum winter air temperatures were captured by introducing an additional density-independent mortality term μ_c, that increased when the annual minimum air temperature within a grid cell, T_{min}, specified from the VEMAP2 climatological dataset (Kittel *et al*., 1997), fell below PFT-specific temperature

parameter t_{min} specified from the measurements of Saki (1973)

$$\mu_c = \begin{cases} 0 & \text{if } T_{min} > (t_{min} + 5), \\ \left(1 - \frac{T_{min} - t_{min}}{5}\right) & \text{if } (t_{min} + 5) \geq T_{min}, \geq t_{min} \\ 1.0 & \text{if } T_{min} < t_{min}. \end{cases} \quad \text{(B4)}$$

Recruitment

As in the original ED formulation, recruitment is governed by the allocation of fixed carbon to reproduction. Reflecting the delayed sexual maturity found in forest trees (Nobel & Slayter, 1980), allocation to reproduction only occurred in trees larger than 5 m in height. Seed dispersal was partitioned between local (within gap) and global (all areas within the same grid-cell). The fractions of local and global seed dispersal for each PFT (see Table 1) were determined from the dispersal kernel estimates for relevant canonical species (Pacala *et al*., 1996).

Appendix C: land-use and forest harvesting scenarios

The rates of change in the fraction of agricultural land in each $1^\circ \times 1^\circ$ grid-cell were computed from Waisenen and Bliss (2002) county level dataset of the fraction of land in agricultural use between 1760 and 1990. The data was converted to a $1^\circ \times 1^\circ$ grid by computing area-weighted averages of the values for each of the counties, and portions of counties contained within each grid cell. The rate of change in agricultural fraction was calculated as the difference in agricultural fraction between successive time intervals, and thus only clearing or abandonment happens in a given grid cell within a given time interval. After 1990, the agricultural fraction within a grid cell was assumed to be fixed; however, the relative proportion of primary and secondary vegetation continues to change as secondary vegetation transitions to the primary vegetation land-use class through natural disturbance, and primary vegetation transitions to secondary vegetation through forest harvesting.

Forest harvesting

The forest harvesting scenario used historical statistics of the domestic wood production, accounting for both nonindustrial and industrial wood products using procedures similar to those used by Houghton & Hackler (2000) and Hurtt *et al*. (2002). Fuelwood production in the period 1630–1920 was specified from Reynolds & Pierson (1942), while lumber production between 1799 and 1955 was specified from the data of Hair (1958) and the US Bureau of the Census (1997). For the period 1962–2002 we used national data from FAO (2004) and using USDA Forest Service data (Haynes 2003) to disaggregate the national total between regions in each decade. Because of the different data sources, different supply regions were used for the periods 1700–1960 and 1961–2100. Projections beyond 2002 were based on Haynes (2003). These datasets were combined to produce a time series of timber production subdivided into supply areas and forest product types.

The corresponding removals of aboveground biomass were estimated by converting forest products into round-wood equivalents, and converting wood volumes to biomass using an average density of 0.45 for conifers and 0.65 for hardwoods (Houghton & Hackler, 2000), and assuming an average harvesting efficiency of 0.7 for lumber and 0.9 for pulp and firewood.

The regional biomass harvesting rates were then disaggregated into time-dependent biomass harvesting rates for each grid-cell level based on the relative amount of forest biomass in the different grid-cells within each supply region. Harvesting targets were met by preferential harvesting of mature primary vegetation (primary vegetation with gap age >50 years), followed by mature secondary vegetation (area over 50 years of age originating from agricultural abandonment and plantations over 25 years of age), and finally immature secondary and primary vegetation. The occurrence of plantations was defined by FIA observations of where plantations currently occur (primarily southern regions). In these grid-cells, areas abandoned or harvested after 1960 were planted with southern pines.